

The Landslide Velocity

Shiva P. Pudasaini^{a,b}, Michael Krautblatter^a

^a Technical University of Munich, Chair of Landslide Research
Arcisstrasse 21, D-80333, Munich, Germany

^b University of Bonn, Institute of Geosciences, Geophysics Section
Meckenheimer Allee 176, D-53115, Bonn, Germany

E-mail: shiva.pudasaini@tum.de

Abstract: Proper knowledge of velocity is required in accurately determining the enormous destructive energy carried by a landslide. We present the first, simple and physics-based general analytical landslide velocity model that simultaneously incorporates the internal deformation (non-linear advection) and externally applied forces, consisting of the net driving force and the viscous resistant. From the physical point of view, the model stands as a novel class of non-linear advective – dissipative system where classical Voellmy and inviscid Burgers' equation are specifications of this general model. We show that the non-linear advection and external forcing fundamentally regulate the state of motion and deformation, which substantially enhances our understanding of the velocity of a coherently deforming landslide. Since analytical solutions provide the fastest, the most cost-effective and the best rigorous answer to the problem, we construct several new and general exact analytical solutions. These solutions cover the wider spectrum of landslide velocity and directly reduce to the mass point motion. New solutions bridge the existing gap between the negligibly deforming and geometrically massively deforming landslides through their internal deformations. This provides a novel, rapid and consistent method for efficient coupling of different types of mass transports. The mechanism of landslide advection, stretching and approaching to the steady-state has been explained. We reveal the fact that shifting, up-lifting and stretching of the velocity field stem from the forcing and non-linear advection. The intrinsic mechanism of our solution describes the fascinating breaking wave and emergence of landslide folding. This happens collectively as the solution system simultaneously introduces downslope propagation of the domain, velocity up-lift and non-linear advection. We disclose the fact that the domain translation and stretching solely depends on the net driving force, and along with advection, the viscous drag fully controls the shock wave generation, wave breaking, folding, and also the velocity magnitude. This demonstrates that landslide dynamics are architected by advection and reigned by the system forcing. The analytically obtained velocities are close to observed values in natural events. These solutions constitute a new foundation of landslide velocity in solving technical problems. This provides the practitioners with the key information in instantly and accurately estimating the impact force that is very important in delineating hazard zones and for the mitigation of landslide hazards.

1 Introduction

There are three methods to investigate and solve a scientific problem: laboratory or field data, numerical simulations of governing complex physical-mathematical model equations, or exact analytical solutions of simplified model equations. This is also the case for mass movements including extremely rapid flow-type landslides **processes** such as debris avalanches (Pudasaini and Hutter, 2007). The dynamics of a landslide are primarily controlled by the flow velocity. Estimation of the flow velocity is key for assessment of landslide hazards, design of protective structures, mitigation measures and landuse planning (Tai et al., 2001; Pudasaini and Hutter, 2007; Johannesson et al., 2009; Christen et al., 2010; Dowling and Santi, 2014; Cui et al., 2015; Faug, 2015; Kattel et al., 2018). Thus, a proper understanding of landslide velocity is a crucial requirement for an appropriate modelling of landslide impact force because the associated hazard is directly and strongly related to the landslide velocity (Huggel et al., 2005; Evans et al., 2009; Dietrich and Krautblatter, 2019). **So, the landslide velocity is of great theoretical and practical interest for both scientists and engineers.** However, the mechanical controls of the evolving velocity, runout and impact energy of the landslide have not yet been understood well.

45 Due to the complex terrain, infrequent occurrence, and very high time and cost demands of field measurements,
46 the available data on landslide dynamics are insufficient. Proper understanding and interpretation of the data
47 obtained from the field measurements are often challenging because of the very limited nature of the material
48 properties and the boundary conditions. Additionally, field data are often only available for single locations
49 and determined as static data after events. Dynamic data are rare (de Haas et al., 2020). So, much of the low
50 resolution measurements are locally or discretely based on points in time and space (Berger et al., 2011; Schürch
51 et al., 2011; McCoy et al., 2012; Theule et al., 2015; Dietrich and Krautblatter, 2019). Therefore, laboratory
52 or field experiments (Iverson et al., 2011; de Haas and van Woerkom, 2016; Lu et al., 2016; Lanzoni et al.,
53 2017, Li et al., 2017; Pilvar et al., 2019; Baselt et al., 2021) and theoretical modelling (Le and Pitman, 2009;
54 Pudasaini, 2012; Pudasaini and Mergili, 2019) remain the major source of knowledge in landslide and debris
55 flow dynamics. Recently, there has been a rapid increase in the comprehensive numerical modelling for mass
56 transports (McDougall and Hungr, 2005; Medina et al., 2008; Cascini et al., 2014; Cuomo et al., 2016; Frank
57 et al., 2015; Iverson and Ouyang, 2015; Mergili et al., 2020a,b; Qiao et al., 2019; Liu et al. 2021). However,
58 to certain degree, numerical simulations are approximations of the physical-mathematical model equations.
59 **Although numerical simulations may overcome the limitations in the measurements and facilitate for a more**
60 **complete understanding by investigating much wider aspects of the flow parameters, run-out and deposition,**
61 **Their usefulness is of such simulations are** often evaluated empirically (Mergili et al., 2020a, 2020b). In contrast,
62 exact, analytical solutions (Faug et al., 2010; Pudasaini, 2011) can provide better insights into the complex
63 flow behaviors, mainly the velocity. **, and their consequences.** Moreover, analytical and exact solutions to
64 non-linear model equations are necessary to elevate the accuracy of numerical solution methods (Chalfen and
65 Niemiec, 1986; Pudasaini, 2011, 2016; Pudasaini et al., 2018). For this reason, here, we are mainly concerned
66 in presenting exact analytical solutions for the newly developed general landslide velocity **model** equation.

67 Since Voellmy's pioneering work, several analytical models and their solutions have been presented in the liter-
68 ature for mass movements including extremely rapid flow-type landslide processes, avalanches and debris flows
69 (Voellmy, 1955; Salm, 1966; Perla et al., 1980; McClung, 1983). However, on the one hand, all these solutions
70 are effectively simplified to the mass point or center of mass motion. None of the existing analytical velocity
71 models consider advection or internal deformation. On the other hand, the parameters involved in these models
72 only represent restricted physics of the landslide material and motion. Nevertheless, a full analytical model that
73 includes a wide range of essential physics of the mass movements incorporating important process of internal
74 deformation and motion is still lacking. This is required for the more accurate description of landslide mo-
75 tion. **Moreover, recently presented simple analytical solutions for mass transports considered debris avalanches**
76 **(Pudasaini, 2011), two-phase flows (Ghosh Hajra et al., 2017, 2018), landslide mobility (Pudasaini and Miller,**
77 **2013; Parez and Aharonov, 2015), fluid flows in debris materials (Pudasaini, 2016), mud flow (Di Cristo et al.,**
78 **2018), granular front down an incline (Saingier et al., 2016), granular monoclinical wave (Razis et al., 2018) and**
79 **the submarine debris flows (Rui and Yin, 2019). However, neither a more general landslide model as we have**
80 **derived here, nor the solution for such a model exists in literature.**

81 **In the recent years, different analytical solutions have been presented for mass transports. These include sim-**
82 **ple and reduced analytical solutions for avalanches and debris flows (Pudasaini, 2011), two-phase flows (Ghosh**
83 **Hajra et al., 2017, 2018), landslide and avalanche mobility (Pudasaini and Miller, 2013; Parez and Aharonov,**
84 **2015), fluid flows in porous and debris materials (Pudasaini, 2016), flow depth profiles for mud flow (Di Cristo**
85 **et al., 2018), simulating the shape of a granular front down a rough incline (Saingier et al., 2016), the granular**
86 **monoclinical wave (Razis et al., 2018) and the mobility of submarine debris flows (Rui and Yin, 2019). However,**
87 **neither a more general landslide model as we have derived here, nor the solution for such a model exists in**
88 **literature.**

89 **This paper presents a novel non-linear advective - dissipative transport equation with quadratic source term**
90 **representing the system forcing, containing the physical/mechanical parameters as a function of the state vari-**
91 **able (the velocity) and their exact analytical solutions describing the landslide motion. The new landslide**
92 **velocity model and its analytical solutions are more general and constitute the full description for velocities**
93 **with wide range of applied forces and the internal deformation. Importantly, the newly developed landslide**
94 **velocity model covers both the classical Voellmy and inviscid Burgers' equations as special cases, unifies and**

95 extends them further, but it also describes fundamentally novel and broad physical phenomena.

96 This paper presents a novel non-linear advective - dissipative transport equation with quadratic source term as
97 a function of the state variable (the velocity) and their exact analytical solutions describing the landslide motion
98 down a slope. The source term represents the system forcing, containing the physical/mechanical parameters
99 and the landslide velocity. Our dynamical velocity equation largely extends the existing landslide models and
100 range of their validity. The new landslide velocity model and its analytical solutions are more general and
101 constitute the full description for velocities with wide range of applied forces and the internal deformation
102 associated with the spatial velocity gradient. In this form, and with respect to the underlying physics and
103 dynamics, the newly developed landslide velocity model covers both the classical Voellmy and inviscid Burgers
104 equation as special cases, but it also describes fundamentally novel and broad physical phenomena. Import-
105 antly, the new model unifies the Voellmy and inviscid Burgers' models and extends them further.

106 It is a challenge to construct exact analytical solutions even for the simplified problems in mass transport
107 (Pudasaini, 2011, 2016; Di Cristo et al., 2018; Pudasaini et al., 2018). In its full form, this is also true for
108 the landslide velocity model developed here. In contrast to the existing models, such as Voellmy-type and
109 Burgers-type, the great complexity in solving the new landslide velocity model equation analytically derives
110 from the simultaneous presence of the internal deformation (non-linear advection, inertia) and the quadratic
111 source representing externally applied forces (in terms of velocity, including physical parameters). However,
112 here, we constructing advance further by constructing However, here, we construct various analytical and exact
113 solutions to the new general landslide velocity model by applying different advanced mathematical techniques,
114 including those presented by Nadjafikhah (2009) and Montecinos (2015). We revealed several major novel
115 dynamical aspects associated with the general landslide velocity model and its solutions. We show that a
116 number of important physical phenomena are captured by the new solutions. Some special features of the new
117 solutions are discussed in detail. This includes - landslide propagation and stretching; wave generation and
118 breaking; and landslide folding. We also observed that different methods consistently produce similar analytical
119 solutions. This highlights the intrinsic characteristics of the landslide motion described by our new model. As
120 exact, analytical solutions disclose many new and essential physics, the solutions derived in this paper may
121 find applications in environmental, engineering and industrial mass transport down slopes and channels.

122 2 Basic Balance Equation for Landslide Motion

123 2.1 Mass and momentum balance equations

124 A geometrically two-dimensional motion down a slope is considered. Let t be time, (x, z) be the coordinates
125 and (g^x, g^z) the gravity accelerations along and perpendicular to the slope, respectively. Let, h and u be the
126 flow depth and the mean flow velocity along the slope. Similarly, γ, α_s, μ be the density ratio between the fluid
127 and the particles ($\gamma = \rho_f/\rho_s$), volume fraction of the solid particles (coarse and fine solid particles), and the
128 basal friction coefficient ($\mu = \tan \delta$), where δ is the basal friction angle, in the mixture material. Furthermore,
129 K is the earth pressure coefficient as a function of internal and the basal friction angles, and C_{DV} is the viscous
130 drag coefficient.

131 We start with the multi-phase mass flow model (Pudasaini and Mergili, 2019) and include the viscous drag
132 (Pudasaini and Fischer, 2020). For simplicity, we first assume that the relative velocity between coarse and
133 fine solid particles (u_s, u_{fs}) and the fluid phase (u_f) in the landslide (debris) material is negligible, that is,
134 $u_s \approx u_{fs} \approx u_f =: u$, and so is the viscous deformation of the fluid. This means, for simplicity, we are considering
135 an effectively single-phase mixture flow. Then, by summing up the mass and momentum balance equations
136 (Pudasaini and Mergili, 2019; Pudasaini and Fischer, 2020), we obtain a single mass and momentum balance
137 equation describing the motion of a landslide as:

$$\frac{\partial h}{\partial t} + \frac{\partial}{\partial x} (hu) = 0, \quad (1)$$

$$\frac{\partial}{\partial t}(hu) + \frac{\partial}{\partial x} \left[hu^2 + (1 - \gamma) \alpha_s g^z K \frac{h^2}{2} \right] = h \left[g^x - (1 - \gamma) \alpha_s g^z \mu - g^z \{1 - (1 - \gamma) \alpha_s\} \frac{\partial h}{\partial x} - C_{DV} u^2 \right], \quad (2)$$

139 where $-(1 - \alpha_s) g^z \partial h / \partial x$ emerges from the hydraulic pressure gradient associated with possible interstitial
 140 fluids in the landslide. Moreover, the term containing K on the left hand side, and the other terms on the
 141 right hand side in the momentum equation (2) represent all the involved forces. The first term in the square
 142 bracket on the left hand side of (2) describes the advection, while the second term (in the square bracket)
 143 describes the extent of the local deformation that stems from the hydraulic pressure gradient of the free-
 144 surface of the landslide. The first, second, third and fourth terms on the right hand side of (2) are the gravity
 145 acceleration; effective Coulomb friction which includes lubrication $(1 - \gamma)$, liquefaction (α_s) (because, if there is
 146 no or substantially low amount of solid, the mass is fully liquefied, e.g., lahar flows); **the local deformation due**
 147 **to the pressure gradient the term associated with buoyancy and the fluid-related hydraulic pressure gradient**;
 148 and the viscous drag, respectively. Note that the term with $1 - \gamma$ or γ originates from the buoyancy effect. By
 149 setting $\gamma = 0$ and $\alpha_s = 1$, we obtain a dry landslide, grain flow or an avalanche motion. For this choice, the
 150 third term on the right hand side vanishes. However, we keep γ and α_s also to include possible fluid effects in
 151 the landslide (mixture).

152 2.2 The landslide velocity equation

153 The momentum balance equation (2) can be re-written as:

$$\begin{aligned} & h \left[\frac{\partial u}{\partial t} + u \frac{\partial u}{\partial x} \right] + u \left[\frac{\partial h}{\partial t} + \frac{\partial}{\partial x} (hu) \right] \\ & = h \left[g^x - (1 - \gamma) \alpha_s g^z \mu - g^z \{((1 - \gamma) K + \gamma) \alpha_s + (1 - \alpha_s)\} \frac{\partial h}{\partial x} - C_{DV} u^2 \right]. \end{aligned} \quad (3)$$

154 Note that for $K = 1$ (which mostly prevails for extensional flows, Pudasaini and Hutter, 2007), the third term
 155 on the right hand side associated with $\partial h / \partial x$ simplifies drastically, because $\{((1 - \gamma) K + \gamma) \alpha_s + (1 - \alpha_s)\}$
 156 becomes unity. So, the isotropic assumption (i.e., $K = 1$) loses some important information about the solid
 157 content and the buoyancy effect in the mixture. Employing the mass balance equation (1), the momentum
 158 balance equation (3) can be re-written as:

$$\frac{\partial u}{\partial t} + u \frac{\partial u}{\partial x} = g^x - (1 - \gamma) \alpha_s g^z \mu - g^z \{((1 - \gamma) K + \gamma) \alpha_s + (1 - \alpha_s)\} \frac{\partial h}{\partial x} - C_{DV} u^2. \quad (4)$$

159 The gradient $\partial h / \partial x$ might be approximated, say as h_g , and still include its effect as a parameter that may be
 160 estimated. Here, we are mainly interested in developing a simple but more general landslide velocity model
 161 than the existing ones that can be solved analytically and highlight its essence to enhance our understanding
 162 of the landslide dynamics.

163 Now, with the notation $\alpha := g^x - (1 - \gamma) \alpha_s g^z \mu - g^z \{((1 - \gamma) K + \gamma) \alpha_s + (1 - \alpha_s)\} h_g$, which includes the forces:
 164 gravity; friction, lubrication and liquefaction; and surface gradient; and $\beta := C_{DV}$, which is the viscous drag
 165 coefficient, (4) becomes a simple model equation:

$$\frac{\partial u}{\partial t} + u \frac{\partial u}{\partial x} = \alpha - \beta u^2, \quad (5)$$

166 where α and β constitute the net driving and the resisting forces in the system. We call (5) the landslide
 167 velocity equation.

168 2.3 A novel physical–mathematical system

169 Equation (5) constitutes a **genuinely** novel class of non-linear advective - dissipative system and involves dynamic
 170 interactions between the non-linear advective (or, inertial) term $u \partial u / \partial x$ and the external forcing (source) term

171 $\alpha - \beta u^2$. However, in contrast to the viscous Burgers' equation where the dissipation is associated with the
 172 (viscous) diffusion, here, dissipation stems because of the viscous drag, $-\beta u^2$. In the form, (5) is similar to the
 173 classical shallow water equation. However, from the mechanics and the material composition, it is much wider
 174 as such model does not exist in the literature. From the physical and mathematical point of view, there are
 175 two crucial novel aspects associated with model (5). First, it explains the dynamics of deforming landslide and
 176 thus extends the classical Voellmy model (Voellmy, 1955; Salm, 1966; McClung, 1983; Pudasaini and Hutter,
 177 2007) due to the broad physics carried by the model parameters, α, β ; and the dynamics described by the new
 178 term $u\partial u/\partial x$. These parameters and the term $u\partial u/\partial x$ control the landslide deformation and motion. Second,
 179 it extends the classical non-linear inviscid Burgers' equation by including the non-linear source term, $\alpha - \beta u^2$,
 180 as a quadratic function of the unknown field variable, u , taking into account many different forces. associated
 181 with the system as explained in Section 2.2.

182 From the structure, (5) is a fundamental non-linear partial differential equation, or a non-linear transport
 183 equation with a source, where the source is the external physical forcing. Such an equation explains the non-
 184 linear advection with source term that contains the physics of the underlying problem through the parameters
 185 α and β . The form of this equation is very important as it may describe the dynamical state of many extended
 186 (as compared to the Voellmy and Burgers models) physical and engineering problems appearing in nature,
 187 science and technology, including viscous/fluid flow, traffic flow, shock theory, gas dynamics, landslide and
 188 avalanches (Burgers, 1948; Hopf, 1950; Cole, 1951; Nadjafikhah, 2009; Pudasaini, 2011; Montecinos, 2015).

189 3 The Landslide Velocity: Simple Solutions

190 Exact analytical solutions to simplified cases of non-linear debris avalanche model equations provide important
 191 insight into the full behavior of the system, and are necessary to calibrate numerical simulations. of flow depth
 192 and velocity profiles. These problem-specific solutions provide important insight into the full behavior of the
 193 system. Physically meaningful exact solutions explain the true and entire nature of the problem associated with
 194 the model equation, and thus, are superior over numerical simulations (Pudasaini, 2011; Faug, 2015). Physically
 195 meaningful exact solutions explain the true and entire nature of the problem associated with the model equation
 196 (Pudasaini, 2011; Faug, 2015), and thus, should be developed, analyzed and properly understood prior to
 197 numerical simulations. These exact analytical solutions provide important insights into the full flow behavior
 198 of the complex system (Pudasaini and Krautblatter, 2021), and are often needed to calibrate and validate the
 199 numerical solutions (Pudasaini, 2016) as a prerequisite before running numerical simulations based on complex
 200 numerical schemes. This is very useful to interpret complicated simulations and/or avoid mistakes associated
 201 with numerical simulations.

202 One of the main purposes of this contribution is to obtain exact analytical velocities for the landslide model (5).
 203 In the form (5) is simple. So, one may tempt to solve it analytically to explicitly obtain the landslide velocity.
 204 However, it poses a great mathematical challenge to derive explicit analytical solutions for the landslide velocity,
 205 u . This is mainly due to the new terms appearing in (5). Below, we construct five different exact analytical
 206 solutions to the model (5) in explicit form. In order to gain some physical insights into the landslide motion,
 207 The solutions are compared to each other. Equation (5) can be considered in two different ways: steady-state
 208 and transient motions, and both without and with (internal) deformation that is described by the term $u\partial u/\partial x$.

209 3.1 Steady-state motion

210 For a sufficiently long time and sufficiently long slope, the time independent steady-state motion can be devel-
 211 oped. Then, (5) reduces to a simplified equation for the landslide velocity down the entire slope:

$$\frac{\partial}{\partial x} \left(\frac{1}{2} u^2 \right) = \alpha - \beta u^2. \quad (6)$$

212 Equivalently, this also represents a mass point velocity along the slope. Classically, (6) is called the center of
 213 mass velocity of a dry avalanche of flow type (Perla et al., 1980) for $\gamma = 0, \alpha_s = 1, K = 1$, and for negligible
 214 free-surface pressure gradient. This will be discussed in detail at Section 3.2.

215 3.1.1 Negligible viscous drag

216 In situations when the Coulomb friction is dominant and the motion is slow, the viscous drag contribution can
 217 be neglected ($\beta u^2 \approx 0$), e.g., typically the moment after the mass release. Then, the solution to (6) is given by
 218 **(Solution A)**:

$$u(x; \alpha) = \sqrt{2\alpha(x - x_0) + u_0^2}, \quad (7)$$

219 where x is the downslope travel distance, and u_0 is the initial velocity at x_0 (or, a boundary condition). Solution
 220 (7) recovers the landslide velocity obtained by considering the simple energy balance for a mass point in which
 221 only the gravity and simple dry Coulomb frictional forces are considered (Scheidegger, 1973), both of these
 222 forces are included in α . Furthermore, when the slope angle is sufficiently high or close to vertical, (7) also
 223 represents a near free fall landslide or rockfall velocity. for which x changes to the vertical height drop.

224 3.1.2 Viscous drag included

225 In general, depending on the magnitude of the net driving force (that also includes the Coulomb friction), the
 226 viscous drag and the magnitude of the velocity, either α or βu^2 , or both can play important role in determining
 227 the landslide motion. Then, the more general solution for (6) than (7) takes the form **(Solution B)**:

$$u(x; \alpha, \beta) = \sqrt{\frac{\alpha}{\beta} \left[1 - \left(1 - \frac{\beta}{\alpha} u_0^2 \right) \frac{1}{\exp(2\beta(x - x_0))} \right]}, \quad (8)$$

228 where, u_0 is the initial velocity at x_0 . We note that as $\beta \rightarrow 0$, the solution (8) approaches (7). The velocity
 229 given by (8) can be compared to the Voellmy velocity and be used to calculate the speed of an avalanche
 230 (Voellmy, 1955; McClung, 1983). However, the Voellmy model only considers the reduced physical aspects in
 231 which α merely includes the gravitational force due to the slope and the dry Coulomb frictional force. This
 232 has been will be discussed in more detail in Section 3.2. As in (7), the solution (8) can also represent a near
 233 free fall landslide (or rockfall) velocity when the slope angle is sufficiently high, or close to vertical, but now,
 234 it also includes the influence of drag, akin to the sky-jump.

235 It is important to reveal the dynamics of viscous drag in the landslide motion. The major aspect of viscous
 236 drag is to bring the velocity (motion) to a terminal velocity (steady, uniform) for a sufficiently long travel
 237 distance. This is achieved by the following relation obtained from (8):

$$\lim_{x \rightarrow \infty} u = \sqrt{\frac{\alpha}{\beta}} =: u_{Tx}, \quad (9)$$

238 where u_{Tx} stands for the terminal velocity of a deformable mass, or a mass point motion (Voellmy), along the
 239 slope that is often used to calculate the maximum velocity of an avalanche (Voellmy, 1955; McClung, 1983;
 240 Pudasaini and Hutter, 2007).

241 In what follows, unless otherwise stated, we use the plausibly chosen physical parameters for rapid mass
 242 movements: slope angle of about 50° , $\gamma = 1100/2700$, $\alpha_s = 0.65$, $\delta = 20^\circ$ (Mergili et al., 2020a, 2020b;
 243 Pudasaini and Fischer, 2020). This implies the model parameters $\alpha = 7.0$, $\beta = 0.0019$. In reality, based
 244 on the physics of the material and the flow, the numerical values of these model parameters should be set
 245 appropriately. However, in principle, all of the results presented here are valid for any choice of the parameter
 246 set $\{\alpha, \beta\}$. For simplicity, $u_0 = 0$ is set at $x_0 = 0$, which corresponds to initially zero velocity at the position
 247 of the mass release. Figure 1 displays the velocity distributions of a landslide down the slope as a function
 248 of the slope position x . The magnitudes of the solutions presented here are mainly for reference purpose. ,
 249 which, however, are subject to scrutiny with laboratory or field data as well as natural events. For the order of
 250 magnitudes of velocities of natural events, we refer to Section 3.2.2. The velocities in Fig. 1 with and without
 251 drag, equations (7) and (8), respectively, behave completely differently already after the mass has moved a
 252 certain distance. For relatively small travel distance, say $x \leq 50$ m, these two solutions are quite similar as
 253 the viscous drag is not sufficiently effective yet. The difference increases rapidly as the mass slides further
 254 down the slope. With the drag, the terminal velocity ($u_{Tx} = \sqrt{\alpha/\beta} \approx 60.1 \text{ m s}^{-1}$) is attained at a sufficient

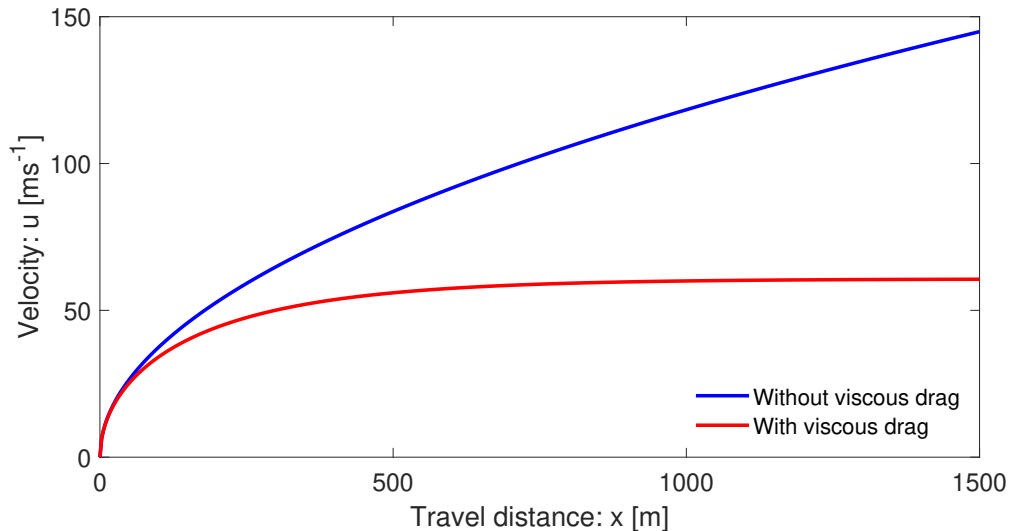


Figure 1: The landslide velocity distributions down the slope as a function of position, for both without and with drag given by (7) and (8), respectively. With drag, the flow attains the terminal velocity $u_{Tx} \approx 60.1 \text{ m s}^{-1}$ at about $x = 600 \text{ m}$, but without drag, the flow velocity increases unboundedly.

255 distance. (about $x = 600 \text{ m}$). But, without drag, the velocity increases forever, which is less likely for a mass
 256 propagating down a long distance.

257 We note that as $\beta \rightarrow 0$, the solution (8) approaches (7). For relatively small travel distance, say $x \leq 50 \text{ m}$,
 258 these two solutions are quite similar as the viscous drag is not sufficiently effective yet. However, for a long
 259 travel distance, $x \gg 50 \text{ m}$, when the viscous drag is not included, the landslide velocity increases steadily
 260 without any control, whilst it increases only slowly, and remains almost unchanged for $x \geq 500 \text{ m}$ when the
 261 viscous drag effect is involved.

262 3.2 A mass point motion

263 Assume no or negligible local deformation (e.g., $\partial u / \partial x \approx 0$), or a Lagrangian description, both are equivalent
 264 to the mass point motion. In this situation, only the ordinary differentiation with respect to time is involved,
 265 and $\partial u / \partial t$ can be replaced by du / dt . Then, the model (5) reduces to

$$\frac{du}{dt} = \alpha - \beta u^2. \quad (10)$$

266 Perla et al. (1980) also called (10) the governing equation for the center of mass velocity, however, for a dry
 267 avalanche of flow type. This is a simple non-linear first order ordinary differential equation. This equation can
 268 be solved to obtain exact analytical solution for the landslide velocity motion in terms of a tangent hyperbolic
 269 function (**Solution C**):

$$u(t; \alpha, \beta) = \sqrt{\frac{\alpha}{\beta}} \tanh \left[\sqrt{\alpha\beta} (t - t_0) + \tanh^{-1} \left(\sqrt{\frac{\beta}{\alpha}} u_0 \right) \right], \quad (11)$$

270 where, $u_0 = u(t_0)$ is the initial velocity at time $t = t_0$. Equation (11) provides the time evolution of the velocity
 271 of the coherent (without fragmentation and substantial deformation) sliding mass until the time it fragments
 272 and/or moves like an avalanche. This transition time is denoted by t_A (or, t_F) indicating fragmentation, or the
 273 inception of the avalanche motion due to fragmentation or large deformation. So, (11) is valid for $t < t_A$. For
 274 $t > t_A$, After that, we must use the full dynamical mass flow model (Pudasaini, 2012; Pudasaini and Mergili,
 275 2019), or the equations (1) and (2). For more detail on it, see Section 6.1. For sufficiently long time, or in the

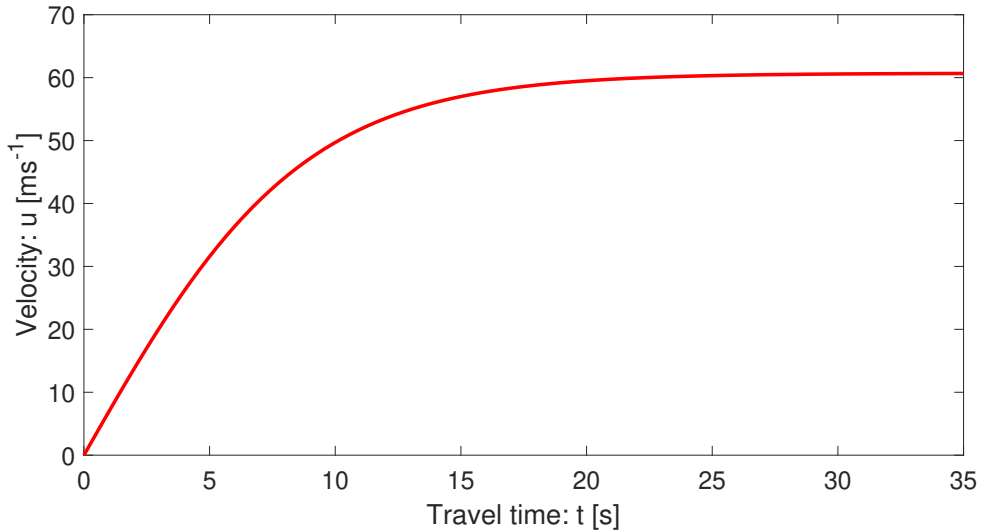


Figure 2: Time evolution of the landslide velocity down the slope with drag given by (11). The motion attains the terminal velocity at about $t = 15$ s.

276 **limit** as the viscous force brings the motion to a non-accelerating state (steady, uniform). Then, from (11) we
 277 obtain:

$$\lim_{t \rightarrow \infty} u = \sqrt{\frac{\alpha}{\beta}} =: u_{Tt}, \quad (12)$$

278 where u_{Tt} stands for the terminal velocity of the motion of a point mass.

279 **The landslide position:** Since $u(t) = dx/dt$, (11) can be integrated to obtain the landslide position as a
 280 function of time:

$$x(t; \alpha, \beta) = x_0 + \frac{1}{\beta} \ln \left[\cosh \left\{ \sqrt{\alpha\beta} (t - t_0) - \tanh^{-1} \left(\sqrt{\frac{\beta}{\alpha}} u_0 \right) \right\} \right] - \frac{1}{\beta} \ln \left[\cosh \left\{ -\tanh^{-1} \left(\sqrt{\frac{\beta}{\alpha}} u_0 \right) \right\} \right], \quad (13)$$

281 where x_0 corresponds to the position at the initial time t_0 . Figure 2 displays the velocity profile of a landslide
 282 **down the slope** as a function of the time as given by (11). **For simplicity, $u_0 = 0$ is set as initial condition at**
 283 **$t_0 = 0$, which corresponds to initially zero velocity at the time of the landslide trigger.** The terminal velocity
 284 ($u_{Tt} = \sqrt{\alpha/\beta}$) is attained at a sufficiently long time (~ 15 s). **We note that,** In the structure, the model (10)
 285 and its solution (11) exists in literature (Pudasaini and Hutter, 2007) and is classically called Voellmy's mass
 286 point model (Voellmy, 1955), or Voellmy-Salm model (Salm, 1966) that disregards the position dependency of
 287 the landslide velocity (Gruber, 1989). But, $(1 - \gamma)$, α_s , and the term associated with h_g are new contributions
 288 and were not included in the Voellmy model, and $K = 1$ therein, while in our consideration α , K can be chosen
 289 appropriately. Thus, the Voellmy model corresponds to the substantially reduced form of α , with $\alpha = g^x - g^z \mu$.

290 3.2.1 The dynamics controlled by the physical and mechanical parameters

291 Solutions (8) and (11) are constructed independently, one for the velocity of a deformable mass as a function
 292 of travel distance, or the velocity of the center of mass of the landslide down the slope, and the other for the
 293 velocity of a mass point motion as a function of time. Unquestionable, they have their own dynamics. However,
 294 for sufficiently long distance and sufficiently long time, or in the space and time limits, these solutions coincide
 295 and we obtain a unique relationship:

$$u_{Tx} = u_{Tt} = \sqrt{\frac{\alpha}{\beta}}. \quad (14)$$

296 So, after a sufficiently long distance or a sufficiently long time, the forces associated with α and β always
 297 maintain a balance resulting in the terminal velocity of the system, $\sqrt{\alpha/\beta}$. This is **remarkable. a fantastic**

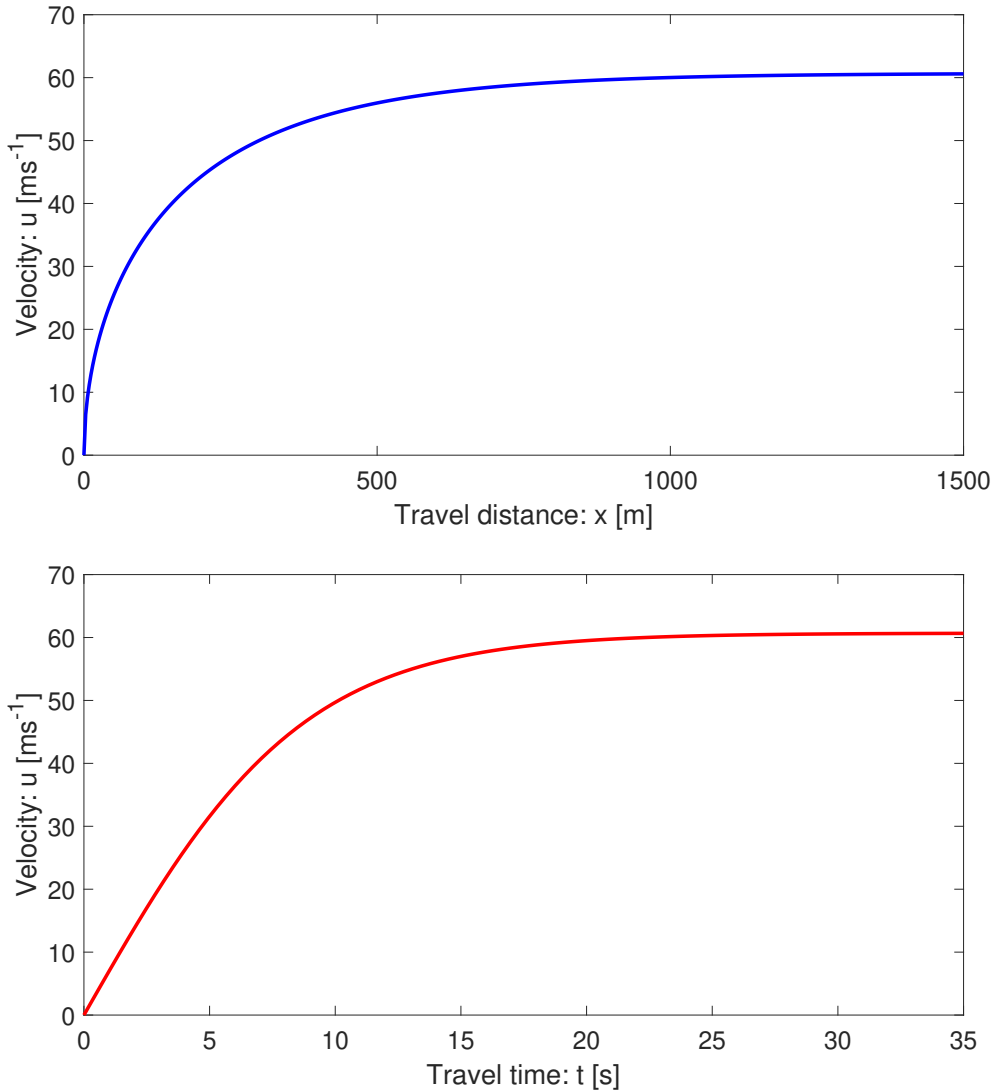


Figure 3: Evolution of the landslide velocity down the slope as a function of space (top) given by (8), and time (bottom) given by (11), respectively, both with drag. The flow attains the terminal velocity at about $x = 600$ m and $t = 15$ s.

298 **situation.** Intuitively this is clear because, one could simply imagine that sufficiently long distance could
 299 somehow be perceived as sufficiently long time, and for these limiting (but fundamentally different) situations,
 300 there exists a single representative velocity that characterizes the dynamics. This has exactly happened, and
 301 is an advanced understanding. This has been shown in Fig. 1 and Fig. 2 which implicitly indicates the
 302 equivalence between (8) and (11). In fact, this can be proven, because, for the mass point or the center of mass
 303 motion,

$$\frac{du}{dt} = \frac{du}{dx} \frac{dx}{dt} = u \frac{du}{dx} = \frac{du}{dx} \left(\frac{1}{2} u^2 \right) = \frac{\partial u}{\partial x} \left(\frac{1}{2} u^2 \right), \quad (15)$$

304 is satisfied.

305 In Fig. 1 and Fig. 2, both velocities (with drag) have the same limiting values. The flow attains the terminal
 306 velocity at about $x = 600$ m and $t = 15$ s, but their early behaviours are quite different. In space, the velocity
 307 shows hyper increase after the incipient motion. However, the time evolution of velocity is slow (almost linear)
 308 at first, then fast, and finally attains the steady-state, $\sqrt{\alpha/\beta} = 60.1$ m s⁻¹, the common value for both the
 309 solutions.

3.2.2 The velocity magnitudes

311 **Importantly, for a uniformly inclined slope, the** Landslide can reach its maximum or the terminal velocity after
312 a relatively short travel distance, or time with value on the order of 50 m s^{-1} . **These are often observed**
313 **scenarios, e.g., for snow or rock-ice avalanches** (Schaerer, 1975; Gubler, 1989; Christen et al., 2002; Havens et
314 al., 2014). The velocity magnitudes presented above are quite reasonable for fast to rapid landslides and debris
315 avalanches **and correspond to several natural events** (Highland and Bobrowsky, 2008). The front of the 2017
316 Piz-Chengalo Bondo landslide (**Switzerland**) moved with more than 25 m s^{-1} already after 20 s of the rock
317 avalanche release (Mergili et al., 2020b), and later it moved at about 50 m s^{-1} (Walter et al., 2020). The 1970
318 rock-ice avalanche event in Nevado Huascarán (**Peru**) reached mean velocity of $50 - 85 \text{ m s}^{-1}$ at about 20 s,
319 but the maximum velocity in the initial stage of the movement reached as high as 125 m s^{-1} (Erismann and
320 Abele, 2001; Evans et al., 2009; Mergili et al. 2018). The 2002 Kolka glacier rock-ice avalanche **in the Russian**
321 **Kaucasus** accelerated with the velocity of about $60 - 80 \text{ m s}^{-1}$, but also attained the velocity as high as 100 m
322 s^{-1} , mainly after the incipient motion (Huggel et al., 2005; Evans et al., 2009).

3.2.3 Accelerating and decelerating motions

324 Depending on the magnitudes of the involved forces, and whether the initial mass was **released or** triggered
325 with a small (including zero) velocity or with high velocity, **e.g., by a strong seismic shacking, e.g., by a strong**
326 **seismic shacking, or when a high potential energy is available and is converted quasi-instantaneously into kinetic**
327 **energy (the situation prevails when the vertical height drop of the detachment area is huge and the slope angle**
328 **of the terrain is high)**, (11) provides fundamentally different but physically meaningful velocity profiles. Both
329 solutions asymptotically approach $\sqrt{\alpha/\beta}$, the lead magnitude in (11). For notational convenience, we write
330 $S_n(\alpha, \beta) = \sqrt{\alpha/\beta}$, which has the dimension of velocity, $\sqrt{\alpha/\beta}$ and is called the separation number (velocity) as
331 it separates accelerating and decelerating regimes. **Description for deceleration is given below.** Furthermore, S_n
332 includes all the involved forces in the system and is the function of the ratio between the mechanically known
333 forces: gravity, friction, lubrication and surface gradient; and the viscous drag force **coefficient**. Thus, S_n fully
334 governs the ultimate state of the landslide motion. For initial velocity less than S_n , i.e., $u_0 < S_n$, the landslide
335 velocity increases rapidly just after its release, then ultimately (after a sufficiently long time) it approaches
336 asymptotically to the steady state, S_n (Fig. 2). This is the accelerating motion. On the other hand, if the initial
337 velocity was higher than S_n , i.e., $u_0 > S_n$, the landslide velocity would decrease rapidly just after its release,
338 then it ultimately would asymptotically approaches to S_n . This is the decelerating motion (not shown here).
339 **We have now two possibilities. First, we can describe $u(t; \alpha, \beta)$ as a function of time with α, β as parameters.**
340 **This corresponds to the velocity profile of the particular landslide characterized by the geometrical, physical**
341 **and mechanical parameters α and β as time evolves. This has been shown in Fig. 2 for $u_0 < S_n$. A similar**
342 **solution can be displayed for $u_0 > S_n$ for which the velocity would decrease and asymptotically approach to**
343 **S_n .**

3.2.4 Velocity described by the space of physical parameters

345 **We have now two possibilities. First, we can describe $u(t; \alpha, \beta)$ as a function of time with α, β as parameters.**
346 **This corresponds to the velocity profile of the particular landslide characterized by the geometrical, physical**
347 **and mechanical parameters α and β as time evolves. This has been shown in Fig. 2. for $u_0 < S_n$. A similar**
348 **solution can be displayed for $u_0 > S_n$ for which the velocity would decrease and asymptotically approach to**
349 **S_n .** Second, we can investigate the control of the physical parameters on the landslide motion for a given
350 time. This is achieved by plotting $u(\alpha, \beta; t)$ as a function of α and β , and considering time as a parameter.
351 Figure 4 shows the influence of **the parameters** α and β on the evolution of the velocity for a landslide motion
352 for a typical time $t = 35 \text{ s}$. The parameters α and β enhance or control the landslide velocity completely
353 differently. For a set of parameters $\{\alpha, \beta\}$, we can now provide an estimate of the landslide velocity. As
354 mentioned earlier, the landslide velocity as high as 125 m s^{-1} have been reported in the literature with their
355 mean and common values in the range of $60 - 80 \text{ m s}^{-1}$ for rapid motions. This way, we can explicitly study
356 the influence of the physical parameters on the dynamics of the velocity field and also determine their range
357 of plausible values. This answers the question on how would the two similar looking, but physically differently

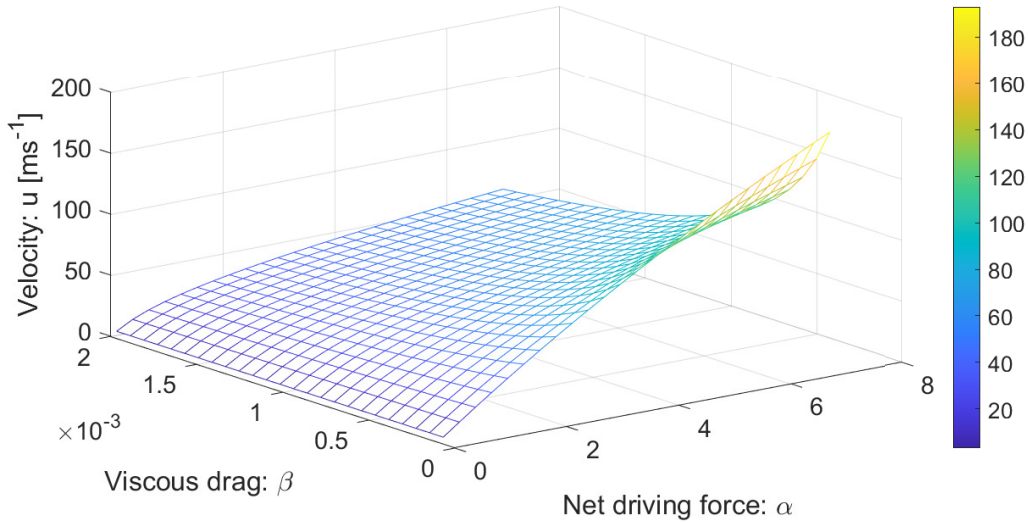


Figure 4: The influence of the model parameters α and β on the landslide velocity. Colorbar shows velocity distributions in m s^{-1} .

358 characterized landslides move. They may behave completely differently.

359 3.2.5 A model for viscous drag

360 There exist explicit models for the interfacial drags between the particles and the fluid (Pudasaini, 2020) in
 361 the multiphase mixture flow (Pudasaini and Mergili, 2019). However, there exists no clear representation
 362 of the viscous drag coefficient for landslide which is the drag between the landslide and the environment.
 363 Often in applications, the drag coefficient ($\beta = C_{DV}$) is prescribed and is later calibrated with the numerical
 364 simulations to fit with the observation or data (Kattel et al., 2016; Mergili et al., 2020a, 2020b). Here, we
 365 explore an opportunity to investigate on how the characteristic landslide velocity (14) offers a **unique** possibility
 366 to define the drag coefficient. Equation (14) can be written as

$$\beta = \frac{\alpha}{u_{max}^2}, \quad (16)$$

367 where, u_{max} represents the maximum possible velocity during the motion as obtained from the (long-time)
 368 steady-state behaviour of the landslide. Equation (16) provides a clear and novel definition (representation) of
 369 the viscous drag in mass movement (flow) as the ratio of the applied forces to the square of the steady-state
 370 (or a maximum possible) velocity the system can attain. With the representative mass m , (16) can be written
 371 as

$$\beta = \frac{\frac{1}{2}m\alpha}{\frac{1}{2}mu_{max}^2}. \quad (17)$$

372 Equivalently, β is the ratio between the one half of the “system-force”, $\frac{1}{2}m\alpha$ (the driving force), and the
 373 (maximum) kinetic energy, $\frac{1}{2}mu_{max}^2$, of the landslide. With the knowledge of the relevant maximum kinetic
 374 energy of the landslide (Körner, 1980), the model (17) for the drag can be closed.

375 3.2.6 Landslide motion down the entire slope

376 Furthermore, we note that following the classical method by Voellmy (Voellmy, 1955) and extensions by Salm
 377 (1966) and McClung (1983), the velocity models (8) and (11) can be used for multiple slope segments to
 378 describe the accelerating and decelerating motions as well as the landslide run-out. These are also called the
 379 release, track and run-out segments of the landslide, or avalanche (Gubler, 1989). However, for the gentle slope,
 380 or the run-out, the frictional force may dominate gravity. In this situation, the sign of α in (5) changes. Then,

381 all the solutions derived above must be thoroughly re-visited with the initial condition for velocity being that
 382 obtained from the lower end of the upstream segment. This way, we can apply the model (5) to analytically
 383 describe the landslide motion for the entire slope, from its release, through the track and the run-out, as well
 384 as to calculate the total travel distance. These methods can also be applied to the general solutions derived in
 385 Section 4 and Section 5.

386 We mention that, for two-dimensional cycloidal or parabolic tracks, Gauer (2018) presented analytical velocities
 387 for the mass block motions with simple dry Coulomb or constant energy dissipation along the track. For such
 388 idealized path geometries he found an important relationship, that the maximum front-velocity, U_{max} , of major
 389 snow avalanches scales with the total drop height of the track, H_{sc} : $U_{max} \sim \sqrt{gH_{sc}/2}$, where g is the gravity
 390 constant. Within its scope, this simple relationship may be applied to estimate the maximum velocity in (17).

391 4 The Landslide Velocity: General Solution - I

392 For shallow motion the velocity may change locally, but the change in the landslide geometry may be param-
 393 eterized. In such a situation, the force produced by the free-surface pressure gradient can be estimated. A
 394 particular situation is the moving slab for which $h_g = 0$, otherwise $h_g \neq 0$. This justifies the physical signifi-
 395 cance of (5).

396 The Lagrangian description of a landslide motion is easier. However, the Eulerian description provides a bet-
 397 ter and more detailed picture of the landslide motion as it also includes the local deformation due to the
 398 velocity gradient. So, here we consider the model equation (5). Without reduction, conceptually, this can
 399 be viewed as an inviscid, non-homogeneous, dissipative Burgers' equation with a quadratic source of system
 400 forces, and includes both the time and space dependencies of u . Exact analytical solutions for (5) can still
 401 be constructed, however, in more sophisticated forms, and is very demanding mathematically. First, For the
 402 notational convenience, we re-write (5) as:

$$\frac{\partial u}{\partial t} + g(u) \frac{\partial u}{\partial x} = f(u), \quad (18)$$

403 where, $g(u) = u$, and $f(u) = \alpha - \beta u^2$ correspond to our model (5). Here, g and f are sufficiently smooth
 404 functions of u , the landslide velocity. Next, We construct exact analytical solution to the generic model (18).
 405 For this, first we state the following theorem from Nadjafikhah (2009).

406 **Theorem 4.1:** *Let f and g be invertible real valued functions of real variables, f is everywhere away from zero,*
 407 *$\phi(u) = \int \frac{1}{f(u)} du$ is invertible, and $l(u) = \int (g(\phi^{-1}(u))) du$. Then, $x = l(\phi(u)) + F[t - \phi(u)]$ is the solution*
 408 *of (18), where F is an arbitrary real valued smooth function of $t - \phi(u)$.*

409 To our problem (5), we have constructed the exact analytical solution (below in Section 4.1), (in Section 4.1),
 410 and reads as (**Solution D**):

$$x = \frac{1}{\beta} \ln \left[\cosh \left(\sqrt{\alpha\beta} \phi(u) \right) \right] + F[t - \phi(u)]; \quad \phi(u) = \frac{1}{2} \frac{1}{\sqrt{\alpha\beta}} \ln \left[\frac{\sqrt{\alpha/\beta} + u}{\sqrt{\alpha/\beta} - u} \right], \quad (19)$$

411 describing the temporal and spatial evolution of the landslide velocity. It is important to note, that in (19),
 412 the major role is played by the function ϕ that contains all the forces of the system. Furthermore, the function
 413 F includes the time-dependency of the solution. The amazing fact with the solution (19) is that any smooth
 414 function F with its argument $[t - \phi(u)]$ is a valid solution of the model equation. This means that, different
 415 landslides may be described by different F functions. Alternatively, a class of landslides might be represented
 416 by a particular function F . This is substantial.

417 4.1 Derivation of the solution to the general model equation

418 Here, we present the detailed derivation of the analytical solution (19) to the landslide velocity equation (5).
 419 We derive the functions ϕ , ϕ^{-1} , l and $l \circ \phi$ that are involved in constructing the analytical solution in Theorem

420 4.1. **for our model (5)**. The first function ϕ is given by

$$\phi(u) = \int \frac{1}{f(u)} du = \int \frac{1}{\alpha - \beta u^2} du = \frac{1}{2\sqrt{\alpha\beta}} \ln \left[\frac{\sqrt{\alpha/\beta} + u}{\sqrt{\alpha/\beta} - u} \right]. \quad (20)$$

421 With the substitution, $\tau = \phi(u)$ (which implies $u = \phi^{-1}(\tau)$), we obtain,

$$\phi^{-1}(\tau) = \sqrt{\frac{\alpha}{\beta}} \left[\frac{\exp(2\sqrt{\alpha\beta}\tau) - 1}{\exp(2\sqrt{\alpha\beta}\tau) + 1} \right] = \sqrt{\frac{\alpha}{\beta}} \tanh(\sqrt{\alpha\beta}\tau). \quad (21)$$

422 So, now the second function ϕ^{-1} can be written in terms of u . However, we must be consistent with the physical
 423 dimensions of the involved variables and functions. The quantities u , $\sqrt{\alpha\beta}$, $\sqrt{\alpha/\beta}$ and τ have dimensions of m
 424 s^{-1} , s^{-1} , $m s^{-1}$ and s. Thus, for the dimensional consistency, the following mapping introduces a new multiplier
 425 λ with the dimension of $1/m s^{-2}$. Therefore, we have

$$\phi^{-1}(u) = \sqrt{\frac{\alpha}{\beta}} \tanh(\sqrt{\lambda\alpha\beta}u). \quad (22)$$

426 With this, the third function $l(u)$ yields:

$$l(u) = \int g(\phi^{-1}(u)) du = \int \phi^{-1}(u) du = \sqrt{\frac{\alpha}{\beta}} \int \tanh(\sqrt{\lambda\alpha\beta}u) du = \frac{1}{\lambda\beta} \ln [\cosh(\lambda\sqrt{\alpha\beta}u)]. \quad (23)$$

427 The fourth function $l(\phi(u)) = (l\phi)(u)$ is instantly achieved:

$$l(\phi(u)) = \left(\frac{\chi}{\lambda}\right) \frac{1}{\beta} \ln [\cosh(\xi\lambda)\sqrt{\alpha\beta}\phi(u)], \quad (24)$$

428 where, as before, the multipliers χ and ξ emerge due to the transformation and for the dimensional consistency,
 429 they have the dimensions of $1/(m s^{-2})$ and $m s^{-2}$, respectively. The nice thing about the groupings (χ/λ) and
 430 $(\xi\lambda)$ is that they are now dimensionless and unity.

431 Utilizing these functions in Theorem 4.1, we finally constructed the exact analytical solution (19). **to the model**
 432 **equation (5) describing the temporal and spatial evolution of the landslide velocity.**

433 4.2 Recovering the mass point motion

434 The amazing fact is that the newly constructed general analytical solution (19) is strong and includes both
 435 the mass point solutions for velocity (11) and the position (13). **Below we prove, that for a special choice of**
 436 **the function F , (19) directly implies both (11) and (13).** For this, consider a particular form of F such that
 437 $F(0) \equiv 0$, which is called a vacuum solution. **First, $F(0) \equiv 0$ which implies that $t = \phi(u)$.** Then, with the
 438 functional relation of $\phi(u)$ in (19), **and after some simple algebraic operations,** we obtain:

$$u = \sqrt{\frac{\alpha}{\beta}} \tanh[\sqrt{\alpha\beta}t]. \quad (25)$$

439 Up to the constant of integration parameters (with $u_0 = 0$ at $t_0 = 0$), (25) is (11). So, the first assertion is
 440 proved. Second, using $F(0) \equiv 0$ and $\phi(u) = t$ in (19), immediately yields

$$x = \frac{1}{\beta} \ln [\cosh(\sqrt{\alpha\beta}t)]. \quad (26)$$

441 Again, up to the constant of integration parameters (with $x_0 = 0$, and $u_0 = 0$ at $t_0 = 0$), (26) is (13). This
 442 proves the second assertion.

443 Moreover, we mention that (25) and (26) can also be obtained formally. This proves that the conditions used
 444 on F are legitimate. To see this, we differentiate (19) with respect to t to yield

$$u = \frac{dx}{dt} = \sqrt{\frac{\alpha}{\beta}} \tanh[\sqrt{\alpha\beta}\phi(u)] \frac{d\phi}{dt} + F'[t - \phi(u)] \left(1 - \frac{d\phi}{dt}\right). \quad (27)$$

445 But, differentiating ϕ in (19) with respect to t and employing (10), we obtain $d\phi/dt = 1$, or $\phi = t$. Now, by
 446 substituting these in (27) and (19) we respectively recover (25) and (26).

447 However, we note that F in (19) is a general function. So, (19) provides a wide spectrum of analytical solutions
 448 for the landslide velocity as a function of time and space, much wider than (11) and (13).

449 4.3 Some particular exact solutions

450 Here, we present some interesting particular exact solutions of (19) in the limit as $\beta \rightarrow 0$. For this purpose,
 451 first we consider (5) with $\beta \rightarrow 0$, and introduce the new variables $\tilde{t} = \alpha t$, $\tilde{x} = \alpha x$. Then, (5) can be written as:

$$\frac{\partial u}{\partial \tilde{t}} + u \frac{\partial u}{\partial \tilde{x}} = 1. \quad (28)$$

452 **Note that each term in this equation is dimensionless.** We apply Theorem 4.1 and the underlying techniques to
 453 (28). So, $f(u) = 1$ implies $\phi(u) = u$, $l(u) = u^2/2$, and $l(\phi(u)) = u^2/2$. Following the procedure as for (19), we
 454 obtain the solution to (28) as: $\tilde{x} = \frac{u^2}{2} + F(\tilde{t} - u)$. However, the direct application of $\phi(u) = u$ in (19) leads
 455 to the solution (that is more complex in its form): $\tilde{x} = \frac{1}{\beta} \ln [\cosh(\sqrt{\beta}u)] + F(\tilde{t} - u)$. Then, in the limit, we
 456 must have:

$$\lim_{\beta \rightarrow 0} \frac{1}{\beta} \ln [\cosh(\sqrt{\beta}u)] = \frac{u^2}{2}. \quad (29)$$

457 This is an important mathematical identity we obtained as a direct consequence of Theorem 4.1 and (19).
 458 Furthermore, the identity (29) when applied to (26) implies:

$$\lim_{\beta \rightarrow 0} x = \lim_{\beta \rightarrow 0} \frac{1}{\beta} \ln [\cosh(\sqrt{\alpha\beta}t)] = \lim_{\beta \rightarrow 0} \frac{1}{\beta} \ln [\cosh\{\sqrt{\beta}(\sqrt{\alpha}t)\}] = \frac{1}{2}\alpha t^2. \quad (30)$$

459 Thus, $x = \frac{1}{2}\alpha t^2$, which is the travel distance in time when the viscous drag is absent. **So, (29) is a physically**
 460 **important identity.**

461 Moreover, with the definition of \tilde{x} , for the particular choice of $F \equiv 0$, $\tilde{x} = \frac{u^2}{2} + F(\tilde{t} - u)$ results in $u(x; \alpha) =$
 462 $\sqrt{2\alpha x}$, which is **the solution given in (7)**. Furthermore, with the choice of $\tilde{x} = 0$, and $F = \tilde{t} - u$, we obtain
 463 $u = 1 - \sqrt{1 - 2\alpha t}$, which for small t , can be approximated as $u \approx \alpha t$. But, in the limit as $\beta \rightarrow 0$, (11) brings
 464 about $u = \alpha t$, which however, is valid for all t values. Thus, (19) generalizes both solutions (7) and (11) in
 465 numerous ways.

466 4.4 Reduction to the classical Burgers' equation

467 Interestingly, by directly taking limit as $\beta \rightarrow 0$, from (19) we obtain

$$x = \frac{u^2}{2\alpha} + F\left(t - \frac{u}{\alpha}\right), \quad (31)$$

468 which can be written as

$$u^2 + 2\alpha F\left(t - \frac{u}{\alpha}\right) - 2\alpha x = 0. \quad (32)$$

469 Importantly, for any choice of the function F , (32) satisfies

$$\frac{\partial u}{\partial t} + u \frac{\partial u}{\partial x} = \alpha, \quad (33)$$

470 which reduces to the classical inviscid Burgers' equation when $\alpha \rightarrow 0$.

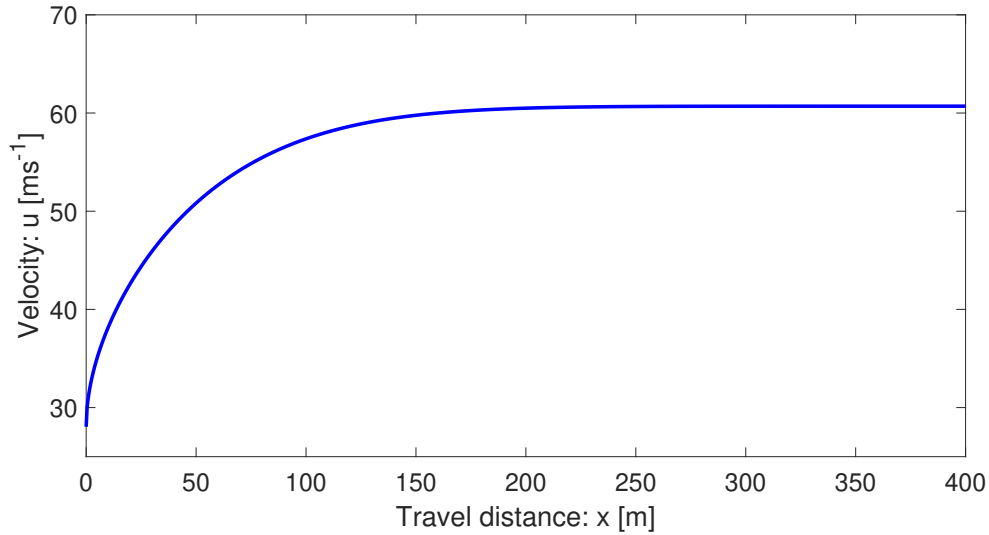


Figure 5: Velocity distribution given by (34).

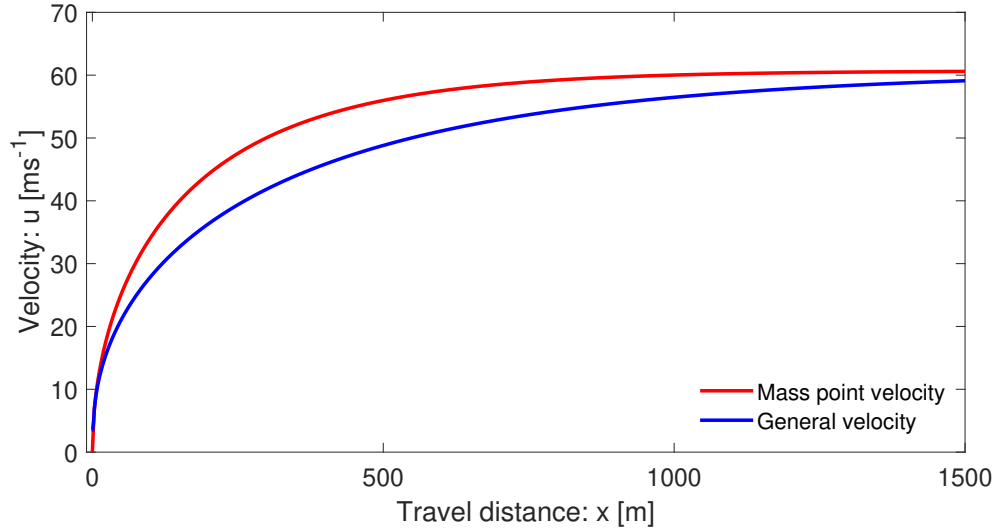


Figure 6: Evolution of the velocity field along the slope as given by (35) for general velocity against the mass point (or, center of mass) velocity corresponding to (8).

471 4.5 Some explicit expressions for u in (19)

472 For a properly selected function F , (19) can be solved exactly for u . For example, consider a constant F ,
 473 $F = \Lambda$. Then, an explicit exact solution is obtained as:

$$u = \sqrt{\frac{\alpha}{\beta}} \tanh \left[\frac{1}{2} \exp \left\{ 2 \cosh^{-1} \left(\exp(\beta(x - \Lambda)) \right) \right\} \right]. \quad (34)$$

474 Figure 5 shows the velocity distribution given by (34) with $u \approx 28 \text{ m s}^{-1}$ at $x = 0$ and $\Lambda = 0$, which reaches
 475 the steady-state at about $x = 150 \text{ m}$, much faster than the solution given by (8) in Fig. 1.

476 However, other more general solutions could be found by considering different F functions in (19). **One such**
 477 **case is presented here.** For example with **the choice** $F = \frac{1}{\beta} \ln \left[c \cosh \left\{ \sqrt{\alpha\beta}(t - \phi(u)) \right\} \right]$, where c is a constant,

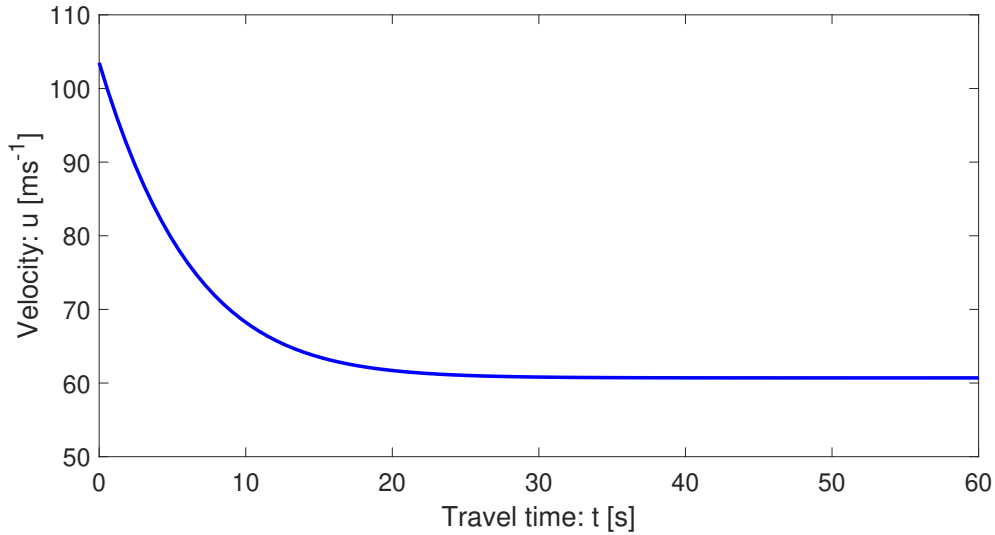


Figure 7: Time evolution of the velocity field as given by (35).

(19) can be solved explicitly for u in terms of x and t : , which, after lengthy algebra, takes the form:

$$u = \sqrt{\frac{\alpha}{\beta}} \tanh \left[\frac{1}{2} \left\{ \cosh^{-1} \left(\frac{2}{c} \exp(\beta x) - \cosh(\sqrt{\alpha\beta} t) \right) + \sqrt{\alpha\beta} t \right\} \right]. \quad (35)$$

The velocity profile along the slope as given by (35) is presented in Fig. 6 for $t = 1 \text{ m s}^{-1}$ and $c = 1$. This solution is quite different to that in Fig. 1 produced by (8). which does not consider the local time variation of the velocity. From the dynamical perspective, the solution (35) is better than the mass point solution (8). The important observation is that the solution given by (8) substantially overestimates the legitimate more general solution (35) that includes both the local time and space variation of the velocity field. The lower velocity with (35) corresponds to the energy consumption due to the deformation associated with the velocity gradient $\partial u / \partial x$ in (5). This will be discussed in more detail in Section 4.5 and Section 4.6. Section 4.6 and Section 4.7.

Furthermore, Fig. 7 presents the time evolution of the velocity field given by (35) for $x = 25 \text{ m}$, $c = -2$. This corresponds to the decelerating flow motion down the slope that starts with a very high velocity and finally asymptotically approaches to the steady-state velocity. of the system. Similar situation has also been discussed at Section 3.2.3, but for a mass point motion.

4.6 Description of the general velocity

A crucial aspect of a complex analytical solution is its proper interpretation. The general solution (19) can be plotted as a function of x and t . the travel distance x and the travel time t . For the purpose of comparing the results with those derived previously, we select F as: $F = [F_k(t - \phi(u))]^{p_w} + F_c$ with parameter values, $F_k = 5000$, $F_c = -500$, $p_w = 1/2$. Furthermore, x is a parameter while plotting the velocity as a function of t . time. In these situations, in order to obtain a physically plausible solution, , the space parameter $x_0 = -600$ is selected. To match the origin of the mass point solution, in plotting, the time has been shifted by -2. Figure 8 depicts the two solutions given by (11) for the mass point motion, and the general solution given by (19) that also includes the internal deformation of the landslide associated with the velocity gradient or the non-linear advection $u \partial u / \partial x$ in (5). They behave essentially differently right after the mass release. The mass point model substantially overestimates landslide velocity derived by the more realistic general model. However, the reduced dimensional models and solutions considered here may give upper bounds to reality because they do not account for the lateral spreading of the landslide mass. Such problems can only be solved comprehensively by considering the numerical simulations on a full three-dimensional digital terrain model (Mergili et al., 2020a,

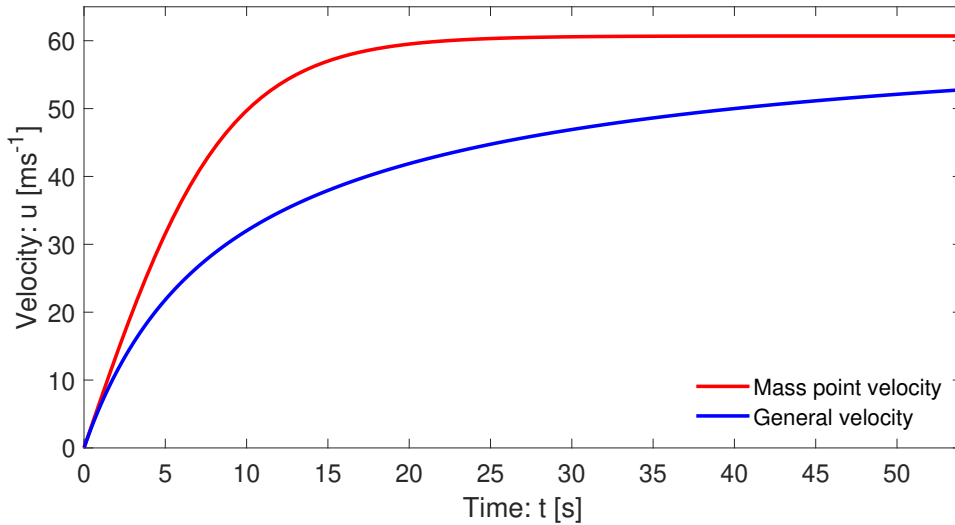


Figure 8: The velocity profiles for a landslide with the mass point motion as given by (11), and the motion including the internal deformation as given by the general solution (19). **The two solutions behave fundamentally differently.**

504 2020b; Shugar et al., 2021) by employing the full dynamical mass flow model equations (Pudasaini and Mergili,
 505 2019) without constraining the lateral spreading.

506 4.7 A fundamentally new understanding

507 The new general solution (19) and its plot in Fig. 8 provides a fundamentally new aspect in our understanding
 508 of landslide velocity. The physics behind the substantially, but legitimately, reduced velocity provided by the
 509 general velocity (19) as compared to the mass point velocity (11) is revealed here for the first time. The gap
 510 between the two solutions increases steadily until a substantially large time (here about $t = 20$ s), then the gap
 511 is reduced slowly. This is so because, after $t = 20$ s the mass point velocity is close to its steady value (about
 512 60.1 m s^{-1}). In the meantime, after $t = 20$ s, the general velocity continues to increase but slowly, and after a
 513 long time, it also tends to approach the steady-state. This substantially lower velocity in the general solution
 514 is realistic. Its mechanism can be explained. It becomes clear by analysing the form of the model equation
 515 (5). For the ease of analysis, we assume the accelerating flow down the slope. For such a situation, both u and
 516 $\partial u/\partial x$ are positive, and thus, $u\partial u/\partial x > 0$. The model (5) can also be written as

$$\frac{\partial u}{\partial t} = (\alpha - \beta u^2) - u \frac{\partial u}{\partial x}. \quad (36)$$

517 Then, from the perspective of the time evolution of u , the last term on the right hand side can be interpreted
 518 as a negative force additional to the system (10) describing the mass point motion. This is responsible for the
 519 substantially reduced velocity profile given by (19) as compared to that given by (11). The lower velocity in
 520 (19) can be perceived as the outcome of the energy consumed in the deformation of the landslide associated
 521 with the spatial velocity gradient that can also be inferred by the negative force attached with $-u\partial u/\partial x$
 522 in (36). Moreover, $u\partial u/\partial x$ in (5) can be viewed as the inertial term of the system (Bertini et al., 1994). However,
 523 after a sufficiently long time the drag is dominant, resulting in the decreased value of $\partial u/\partial x$. Then, the effect
 524 of this negative force is reduced. Consequently, the difference between the mass point solution and the general
 525 solution decreases. However, these statements must be further scrutinized.

526 5 The Landslide Velocity: General Solution - II

527 Below, we have constructed a further exact analytical solution to our velocity equation based on the method
 528 of Montecinos (2015). Consider the model (5) and assign an initial condition:

$$\frac{\partial u}{\partial t} + u \frac{\partial u}{\partial x} = \alpha - \beta u^2, \quad u(x, 0) = s_0(x). \quad (37)$$

529 This is a non-linear advective - dissipative system, and can be perceived as an inviscid, dissipative, non-
 530 homogeneous Burgers' equation. First, we note that, $H(x)$ is a primitive of a function $h(x)$ if $\frac{dH(x)}{dx} = h(x)$.
 531 Then, we summarize the Montecinos (2015) solution method in a theorem:

532 **Theorem 5.1:** Let $\frac{1}{f(u)}$ be an integrable function. Then, there exists a function $\mathcal{E}(t, s_0(y))$ with its primitive
 533 $\mathcal{F}(t, s_0(y))$, such that, the initial value problem

$$\frac{\partial u}{\partial t} + u \frac{\partial u}{\partial x} = f(u), \quad u(x, 0) = s_0(x), \quad (38)$$

534 has the exact solution $u(x, t) = \mathcal{E}(t, s_0(y))$, where y satisfies $x = y + \mathcal{F}(t, s_0(y))$.

535 Following Theorem 5.1, **after a bit lengthy calculation (below in Section 5.1)**, we obtain **(in Section 5.1)** the
 536 exact analytical solution (**Solution E**) for (37):

$$u(x, t) = \sqrt{\frac{\alpha}{\beta}} \tanh \left[\sqrt{\alpha\beta} t + \tanh^{-1} \left\{ \sqrt{\frac{\beta}{\alpha}} s_0(y) \right\} \right], \quad (39)$$

537 where $y = y(x, t)$ is given by

$$x = y + \frac{1}{\beta} \ln \left[\cosh \left\{ \sqrt{\alpha\beta} t + \tanh^{-1} \left\{ \sqrt{\frac{\beta}{\alpha}} s_0(y) \right\} \right\} \right] - \frac{1}{\beta} \ln \left[\cosh \left\{ \tanh^{-1} \left\{ \sqrt{\frac{\beta}{\alpha}} s_0(y) \right\} \right\} \right], \quad (40)$$

538 and, $s_0(x) = u(x, 0)$ provides the functional relation for $s_0(y)$. In contrast to (19), (39)-(40) are the direct
 539 generalizations of the mass point solutions given by (11) and (13). This is an advantage.

540 The solution strategy is as follows: Use the definition of $s_0(y)$ in (40). Then, solve for y . Go back to the
 541 definition of $s_0(y)$ and put $y = y(x, t)$ in $s_0(y)$. This $s_0(y)$ is now a function of x and t . Finally, put
 542 $s_0(y) = f(x, t)$ in (39) to obtain the required general solution for $u(x, t)$. In principle, the system (39)-(40) may
 543 be solved explicitly for a given initial condition. One of the main problems in solving (39)-(40) lies in inverting
 544 (40) to acquire $y(x, t)$. Moreover, we note that, generally, (19) and (39)-(40) may provide different solutions.

545 5.1 Derivation of the solution to the general model equation

546 The solution method involves some sophisticated mathematical procedures. However, here we present a compact
 547 but a quick solution description to our problem. The equivalent ordinary differential equation to the partial
 548 differential equation system (37) is

$$\frac{d\hat{u}}{dt} = \alpha - \beta \hat{u}^2, \quad \hat{u}(0) = s(0), \quad (41)$$

549 which has the solution

$$\hat{u}(t) = \mathcal{E}(t, s(0)) = \sqrt{\frac{\alpha}{\beta}} \tanh \left[\sqrt{\alpha\beta} t + \tanh^{-1} \left\{ \sqrt{\frac{\beta}{\alpha}} s(0) \right\} \right]. \quad (42)$$

550 Consider a curve x in the $x - t$ plane that satisfies the ordinary differential equation

$$\frac{dx}{dt} = \mathcal{E}(t, s_0(y)) = \sqrt{\frac{\alpha}{\beta}} \tanh \left[\sqrt{\alpha\beta} t + \tanh^{-1} \left\{ \sqrt{\frac{\beta}{\alpha}} s_0(y) \right\} \right], \quad x(0) = y. \quad (43)$$

551 Solving the system (43), we obtain,

$$\begin{aligned}
 x &= y + \mathcal{F}(t, s_0(y)) \\
 &= y + \frac{1}{\beta} \ln \left[\cosh \left\{ \sqrt{\alpha\beta} t + \tanh^{-1} \left\{ \sqrt{\frac{\beta}{\alpha}} s_0(y) \right\} \right\} \right] - \frac{1}{\beta} \ln \left[\cosh \left\{ \tanh^{-1} \left\{ \sqrt{\frac{\beta}{\alpha}} s_0(y) \right\} \right\} \right]. \quad (44)
 \end{aligned}$$

552 So, the exact solution to the problem (37) is given by

$$u(x, t) = \mathcal{E}(t, s_0(y)) = \sqrt{\frac{\alpha}{\beta}} \tanh \left[\sqrt{\alpha\beta} t + \tanh^{-1} \left\{ \sqrt{\frac{\beta}{\alpha}} s_0(y) \right\} \right], \quad (45)$$

553 where y satisfies (44).

554 5.2 Recovering the mass point motion

555 It is interesting to observe the structure of the solutions given by (39)-(40). For a constant initial condition,
 556 e.g., $s_0(x) = \lambda_0$, $s_0(y) = \lambda_0$, (39) and (40) are decoupled. Then, (39) reduces to

$$u(x, t) = \sqrt{\frac{\alpha}{\beta}} \tanh \left[\sqrt{\alpha\beta} t + \tanh^{-1} \left(\sqrt{\frac{\beta}{\alpha}} \lambda_0 \right) \right]. \quad (46)$$

557 For $t = 0$, $u(x, 0) = u_0(x) = \lambda_0$, which is the initial condition. Furthermore, (40) takes the form:

$$x = x_0 + \frac{1}{\beta} \ln \left[\cosh \left\{ \sqrt{\alpha\beta} t + \tanh^{-1} \left(\sqrt{\frac{\beta}{\alpha}} \lambda_0 \right) \right\} \right] - \frac{1}{\beta} \ln \left[\cosh \left\{ \tanh^{-1} \left(\sqrt{\frac{\beta}{\alpha}} \lambda_0 \right) \right\} \right], \quad (47)$$

558 from which we see that for $t = 0$, $x = y = x_0$, which is the initial position. With this, we observe that (46) and
 559 (47) are the mass point solutions (11) and (13), respectively.

560 5.3 A particular solution

561 For the choice of the initial condition $s_0(x) = \sqrt{\frac{\alpha}{\beta}} \tanh [\cosh^{-1} \{\exp(\beta x)\}]$, combining (39) and (40) **after a**
 562 **bit of algebra**, leads to

$$u(x, t) = \sqrt{\frac{\alpha}{\beta}} \tanh [\cosh^{-1} \{\exp(\beta x)\}], \quad (48)$$

563 which, surprisingly, is the same as the initial condition. However, we can now legitimately compare (48) with
 564 the previously obtained solution (8), which is the steady-state motion with viscous drag. These two solutions
 565 have been presented in Fig. 9. The very interesting fact is that (8) and (48) turned out to be the same. For a
 566 real valued parameter β and a real variable x , this reveals an important mathematical identity, that

$$\tanh [\cosh^{-1} \{\exp(\beta x)\}] = \sqrt{1 - \exp(-2\beta x)}. \quad (49)$$

567 This means, the very complex function on the left hand side can be replaced by the much simpler function on
 568 the right hand side. Moreover, taking the limit as $\beta \rightarrow 0$ in (48) and comparing it with (7), we obtain another
 569 functional identity:

$$\lim_{\beta \rightarrow 0} \frac{1}{\sqrt{\beta}} \tanh [\cosh^{-1} \{\exp(\beta x)\}] = \sqrt{2x}. \quad (50)$$

570 These identities have mathematical significance.

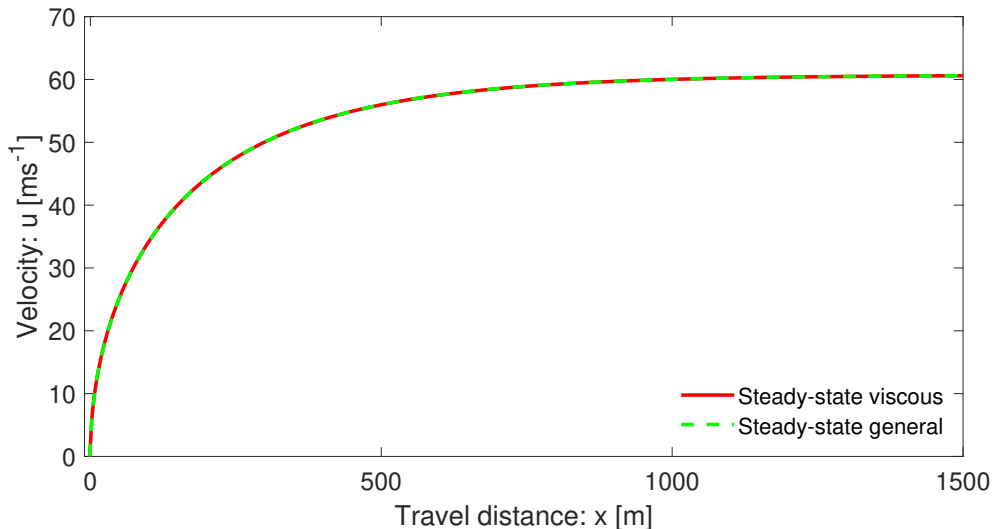


Figure 9: The velocity profile down a slope as a function of position for a landslide given by (39)-(40) reduced to the steady-state (48) against the steady-state solution with viscous drag given by (8). They match perfectly.

5.4 Time marching general solution

Any initial condition can be applied to the solution system (39)-(40). For the purpose of demonstrating the functionality of this system, here we consider two initial conditions: $s_0(x) = x^{0.50}$ and $s_0(x) = x^{0.65}$. The corresponding results are presented in Fig. 10. This figure clearly shows time marching of the landslide motion that also stretches as it slides down. Such deformation of the landslide stems from the term $u\partial u/\partial x$ and the applied forces $\alpha - \beta u^2$ in our primary model (5). We will elaborate on this later. This proves our hypothesis on the importance of the non-linear advection and external forcing on the deformation and motion of the landslide. The mechanism and dynamics of the advection, stretching and approaching to the steady-state can be explained with reference to the general solution. For this, consider the lower panel with initial condition $s_0(x) = x^{0.65}$. At $t = 0.0$ s, (40) implies that $y = x$, then from (39), $u(x, t) = s_0(x)$, which is the initial condition. Such a velocity field can take place in relatively early stage of the developed motion of large natural events (Erismann and Abele, 2001; Huggel et al., 2005; Evans et al., 2009; Mergili et al., 2018). This is represented by the $t = 0.0$ s curve. For the next time, say $t = 2.0$ s, the spatial domain of u expands and shifts to the right as defined by the rule (40). It has three effects in (39). First, due to the shift of the spatial domain, the velocity field u is relocated to the right (downstream). Second, because of the increased t value, and the spatial term associated with \tanh^{-1} , the velocity field is elevated. Third, as the \tanh function defines the maximum value of u (about 60.1 m s^{-1}), the velocity field is controlled (somehow appears to be rotated). This dynamics also applies for $t > 2.0$ s. These jointly produce beautiful spatio-temporal patterns in Fig. 10. Since the maximum of the initial velocity was already close to the steady-state value (the right-end of the curve), the front of the velocity field is automatically and strongly controlled, limiting its value to 60.1 m s^{-1} . So, although the rear velocity increases rapidly, the front velocity remains almost unchanged. After a sufficiently long time, $t \geq 15$ s, the rear velocity also approaches the steady-state value. Then, the entire landslide moves downslope virtually with the constant steady-state velocity, without any substantial stretching. We can similarly describe the dynamics for the upper panel in Fig. 10. However, these two panels reveal an important fact that the initial condition plays an important role in determining and controlling the landslide dynamics.

5.5 Landslide stretching

The stretching (or, deformation) of the landslide propagating down the slope depends on the evolution of its front (x_f) and rear (x_r) positions with maximum and minimum speeds, respectively. This has been shown in Fig. 11 corresponding to the initial condition $s_0(x) = x^{0.65}$ in Fig. 10. It is observed that the rear position

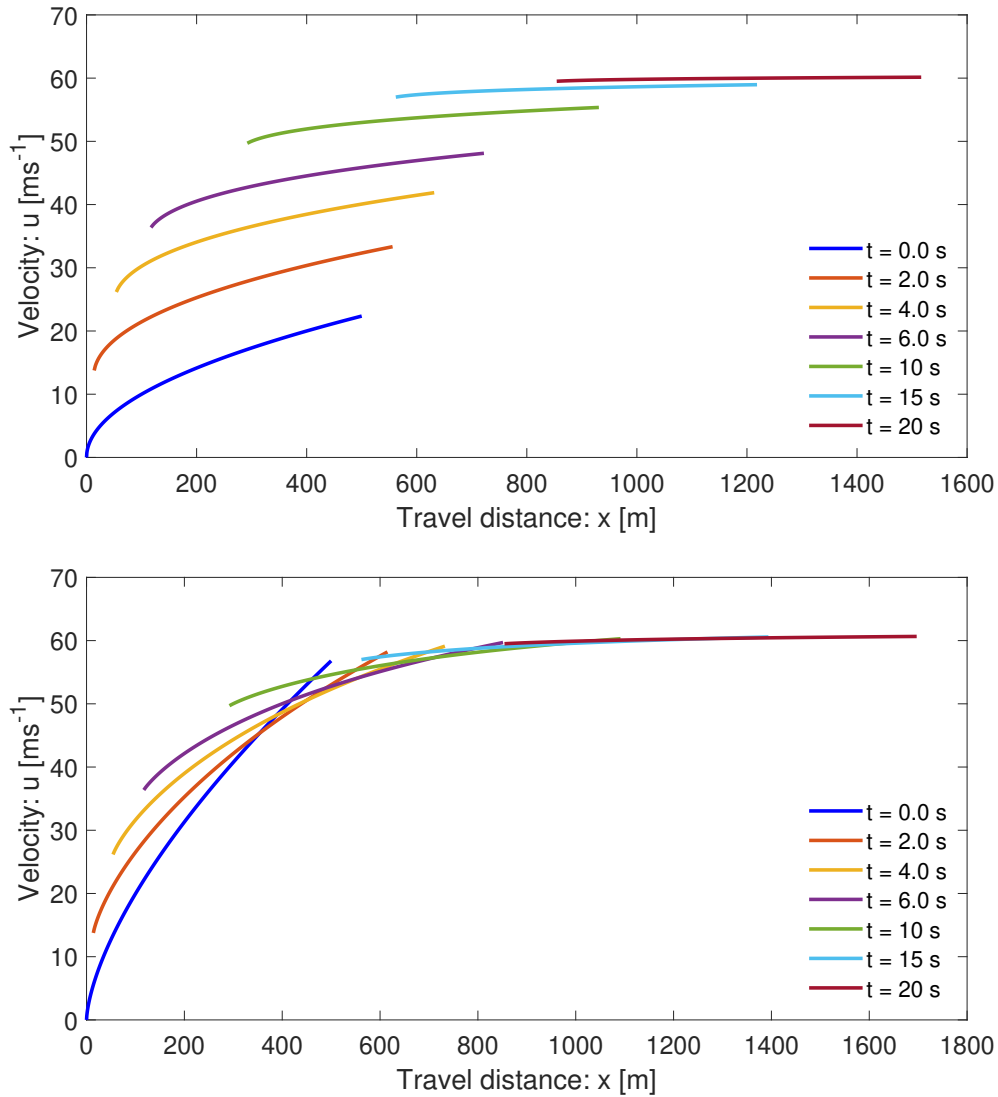


Figure 10: Time evolution of velocity profiles of propagating and stretching landslides down a slope, and as functions of position including the internal deformations as given by the general solution (39)-(40) of (5). The profiles **correspond to evolve based on** the initial conditions $s_0(x) = x^{0.50}$ (top panel, $t = 0.0$ s) and $s_0(x) = x^{0.65}$ (bottom panel, $t = 0.0$ s), respectively.

600 evolves strongly non-linearly whereas the front position advances only weakly non-linearly.

601 In order to better understand the rate of stretching of the landslide, in Fig. 12, we also plot the difference
 602 between the front and rear positions as a function of time. It shows the stretching (rate) of the rapidly
 603 deforming landslide. The stretching dynamics is determined by the front and rear positions of the landslide in
 604 time, as has been shown in Fig. 11. In the early stages, the stretching increases rapidly. However, in later times
 605 (about $t \geq 15$ s) it increases only slowly, and after a sufficiently long time, (the rate of) stretching vanishes
 606 as the landslide has already been fully stretched. **This can be understood, because after a sufficiently long**
 607 **time, the motion is in steady-state. The two panels in Fig. 10 also clearly indicate that the stretching (rate)**
 608 **depends on the initial condition. This can be understood, because after a sufficiently long time, the motion is**
 609 **in steady-state. Nevertheless, the ways the two solutions reach the steady-state are different. The two panels**
 610 **in Fig. 10 also clearly indicate that the stretching (rate) depends on the initial condition.**

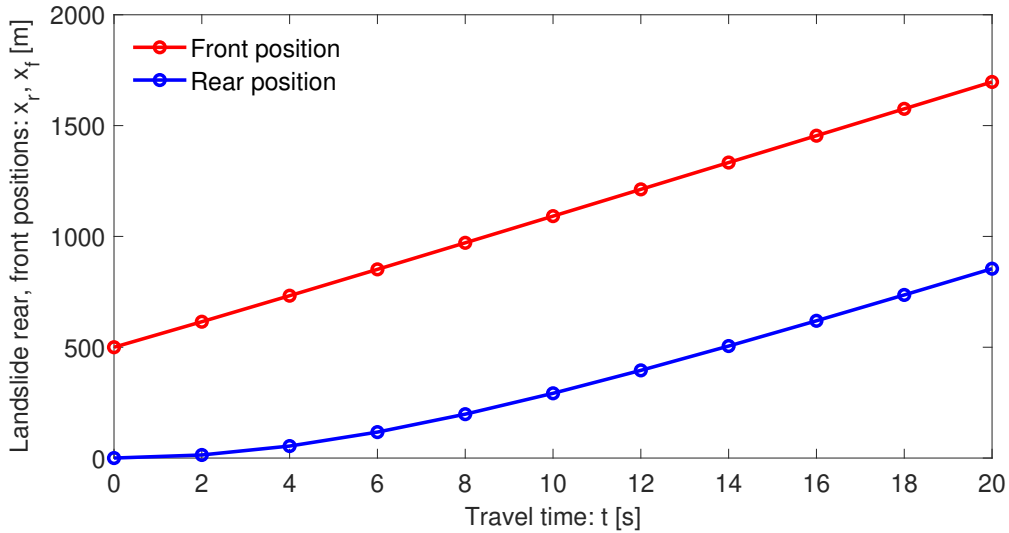


Figure 11: Time evolution of the front and rear positions of the landslide as it moves down the slope including the internal deformation given by the general solution (39)-(40) of (5), corresponding to the initial condition $s_0(x) = x^{0.65}$ in Fig. 10.

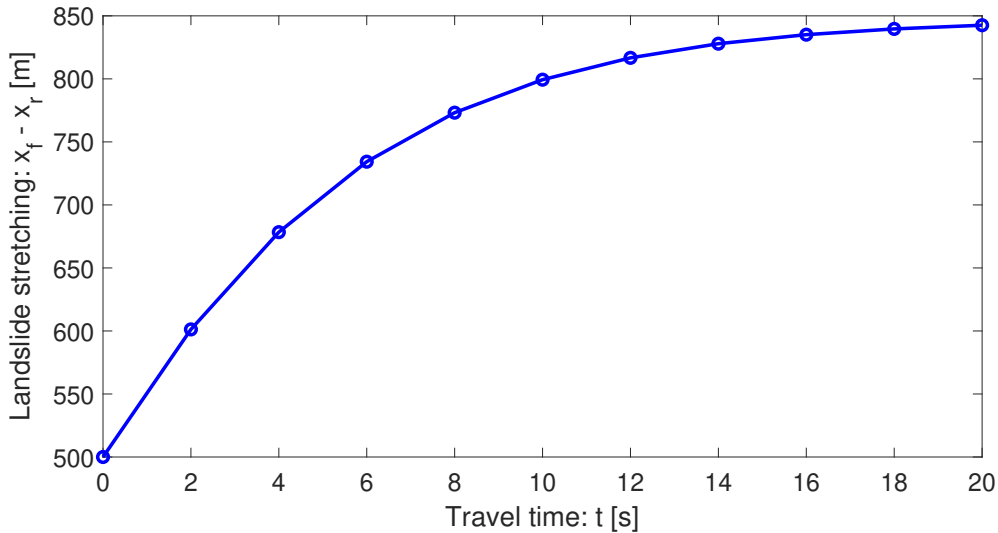


Figure 12: Time stretching of the landslide down the slope including the internal deformation given by the general solution (39)-(40) of (5), corresponding to the initial condition $s_0(x) = x^{0.65}$ in Fig. 10.

5.6 Describing the dynamics

The dynamics observed in Fig. 10 and Fig. 12 can be described with respect to the general model (5) or (37) and its solution given by (39)-(40). The nice thing about (39) is that it can be analyzed in three different ways: with respect to the first or second or both terms on the right hand side. If we disregard the first term involving time, then we explicitly see the effect of the second term that is responsible for the spatial variation of u for each time employed in (40). This results in the shift of the solution for u to the right, and in the mean time, the solution stretches but without changing the possible maximum value of u (not shown). Stretching continues for higher times, however, for a sufficiently long time, it remains virtually unchanged. On the other hand, if we consider both the first and second terms on the right hand side of (39), but use the initial velocity distribution only for a very small x domain, say $[0, 1]$, then, we effectively obtain the mass point solutions

621 given in Fig. 1 and Fig. 2 **top and bottom panels** corresponding to (8) and (11), respectively for the spatial
622 and time evolutions of u . This is so, because now the very small initial domain for x essentially defines the
623 velocity field as if it was for a center of mass motion. Then, as time elapses, the domain shifts to the right and
624 the velocity increases. Now, plotting the velocity field as a function of space and time recovers the solutions in
625 Fig. 1 and Fig. 2. In fact, if we collect all the minimum values of u (the left end points) in Fig. 10 (bottom
626 panel) and plot them in space and time, we acquire both the results in Fig. 1 and Fig. 2. These are effectively
627 the mass point solutions for the spatial and time variation of the velocity field, because these results only focus
628 on the left end values of u , akin to the mass point motion. This means, (40) together with (39) is responsible
629 for the dynamics presented in Fig. 10, Fig. 11 and Fig. 12 corresponding to the term $u\partial u/\partial x$ and $\alpha - \beta u^2$
630 in the general model (5) or (37). So, the dynamics is specially architected by the advection $u\partial u/\partial x$ and
631 controlled by the system forcing $\alpha - \beta u^2$, through the model parameters α and β . This will be discussed in
632 more detail in Section 5.7 - Section 5.9. This is **fascinating, a fantastic situation**, because, it reveals the fact
633 that the shifting, stretching and lifting of the velocity field stems from the term $u\partial u/\partial x$ in (37). After a long
634 time, as drag strongly dominates the other system forces, the velocity approaches the steady-state, practically
635 the velocity gradient vanishes, and thus, the stretching ceases. Then, the landslide just moves down the slope
636 at a constant velocity without any further dynamical complication.

637 5.7 Rolling out the initial velocity

638 It is compelling to see how the solution system (39)-(40) rolls out an initially constant velocity across specific
639 curves. For this, consider an initial velocity $s_0(x) = 0$ in a small domain, say $[0, 3]$, and take a point in it.
640 Then, generate solutions for different times, beginning with $t = 0.0$ s, with 2.0 s increments. As shown in
641 Fig. 13, the space and time evolutions of the velocity fields for a mass point motion given by (8) and (11)
642 have been exactly rolled-up and covered by the system (39)-(40) by transporting the initial velocity along these
643 curves (indicated by the star symbols). As explained earlier, the mechanism is such that, in time, (40) shifts
644 the solution point (domain) to the right and (39) up-lifts the velocity exactly lying on the mass point velocity
645 curves designed by (8) and (11). So, the system (39)-(40) generalizes the mass point motion in many different
646 ways.

647 5.8 Breaking wave and folding

648 Next, we show how the new model (5) and its solution system (39)-(40) can mould the breaking wave in
649 mass transport and describe the folding of a landslide. For this, consider a sufficiently smooth initial velocity
650 distribution given by $s_0(x) = 5 \exp(-x^2/50)$. Such a distribution can be realized, e.g., as the landslide starts
651 to move, its center might have been moving at the maximum initial velocity due to some localized strength
652 weakening mechanism (examples include liquefaction, frictional strength loss; blasting; seismic shaking), and
653 the strength weakening diminishes quickly away from the center. This later leads to a highly stretchable
654 landslide from center to the back, while from center to the front, the landslide contracts strongly. The time
655 evolution of the solution has been presented in Fig. 5.8. The top panel for the usual drag as before ($\beta = 0.0019$),
656 while the bottom panel with higher drag ($\beta = 0.019$). The drag strongly controls the wave breaking and folding,
657 and also the magnitude of the landslide velocity. Here, we focus on the top panel, but similar analysis also
658 holds for the bottom panel.

659 Wave breaking and folding are often observed important dynamical aspects in mass transport and formation
660 of geological structures. Figure 5.8 reveals a thrilling dynamics. The most fascinating feature is the velocity
661 wave breaking and how this leads to the emergence of folding of the landslide. This can be explained with
662 respect to the mechanism associated with the solution system (39)-(40). As $u\partial u/\partial x$ is positive to the left
663 and negative to the right of the maximum initial velocity, the motion to the left of the maximum initial
664 velocity overtakes the velocity to the right of the maximum position. As the position of the maximum velocity
665 accelerates downslope with the fastest speed, after a sufficiently long time, a kink around the front of the
666 velocity wave develops, here after $t = 2$ s. This marks the velocity wave breaking (shock wave formation) and
667 the beginning of the folding. However, the rear stretches continuously. Although mathematically a folding may
668 refer to a singularity due to a multi-valued function, here we explain the folding dynamics as a phenomenon

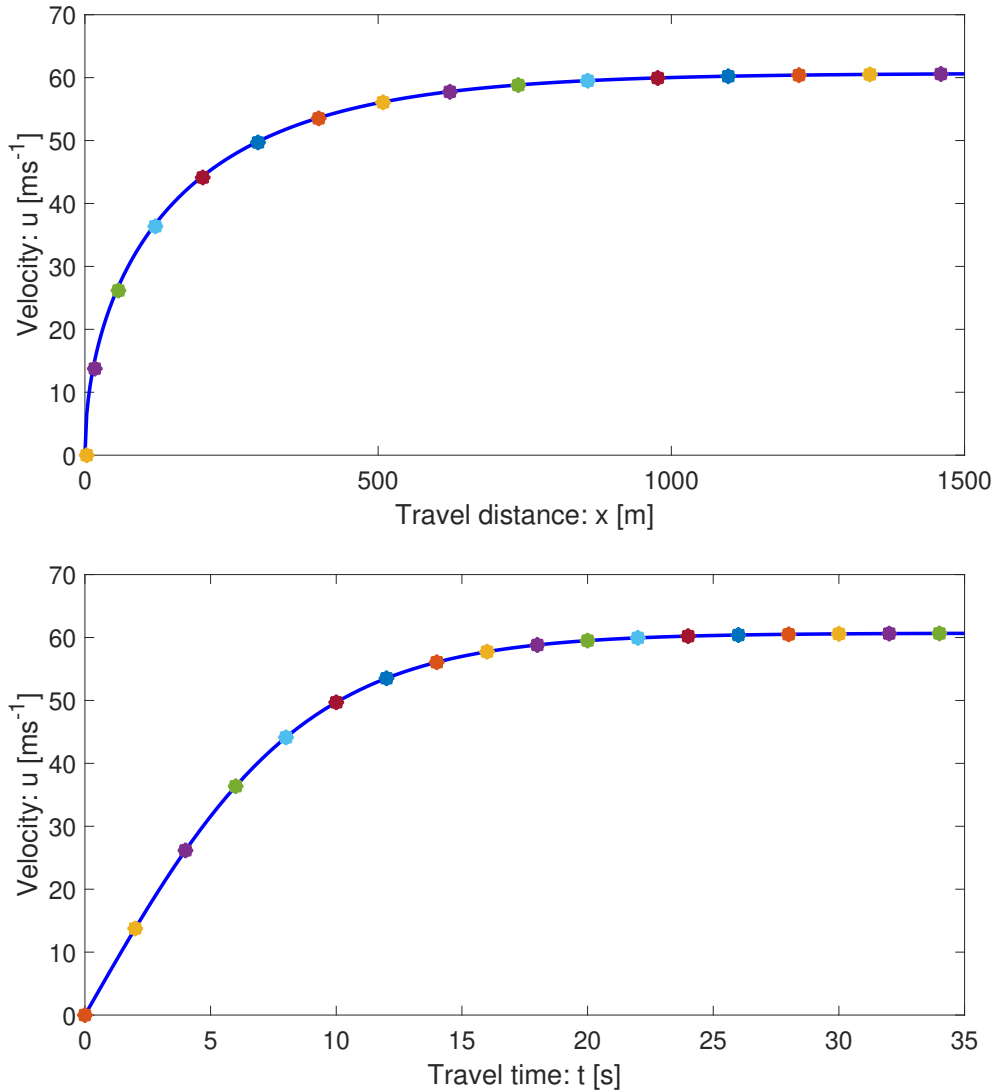


Figure 13: Spatial (top) and temporal (bottom) transportations of the initial velocity ($u = 0$) of the landslide down the slope by the general solution system (39)-(40) as indicated by the star markings for times $t = 0.0$ s, with 2.0 s increments. These solutions exactly fit with the space and time evolutions of the velocity fields (curves) for the mass point motions given by (8) and (11).

669 that can appear in nature. In time, the folding intensifies, the folding length increases, but the folding gap
 670 decreases. After a long time, virtually the folding gap vanishes and the landslide moves downslope at the
 671 steady-state velocity with a perfect fold in the frontal part (not shown), while in the back, it maintains a
 672 single large stretched layer. This happened collectively as the system (39)-(40) simultaneously introduced
 673 three components of the landslide dynamics: downslope propagation, velocity up-lift and breaking or folding in
 674 the frontal part while stretching in the rear. This physically and mathematically proves that the non-uniform
 675 motion (with its maximum somewhere interior to the landslide) is the basic requirement for the development
 676 of the breaking wave and the emergence of landslide folding. **This is a seminal understanding.**

677 5.9 Recovering Burgers' model

678 As the external forcing vanishes, i.e., as $\alpha \rightarrow 0, \beta \rightarrow 0$, the landslide velocity equation (5) reduces to the
 679 classical inviscid Burgers' equation. Then, for $\alpha \rightarrow 0, \beta \rightarrow 0$, one would expect that the general solution
 680 (39)-(40) should also reduce to the formation of the shock wave and wave breaking generated by the inviscid

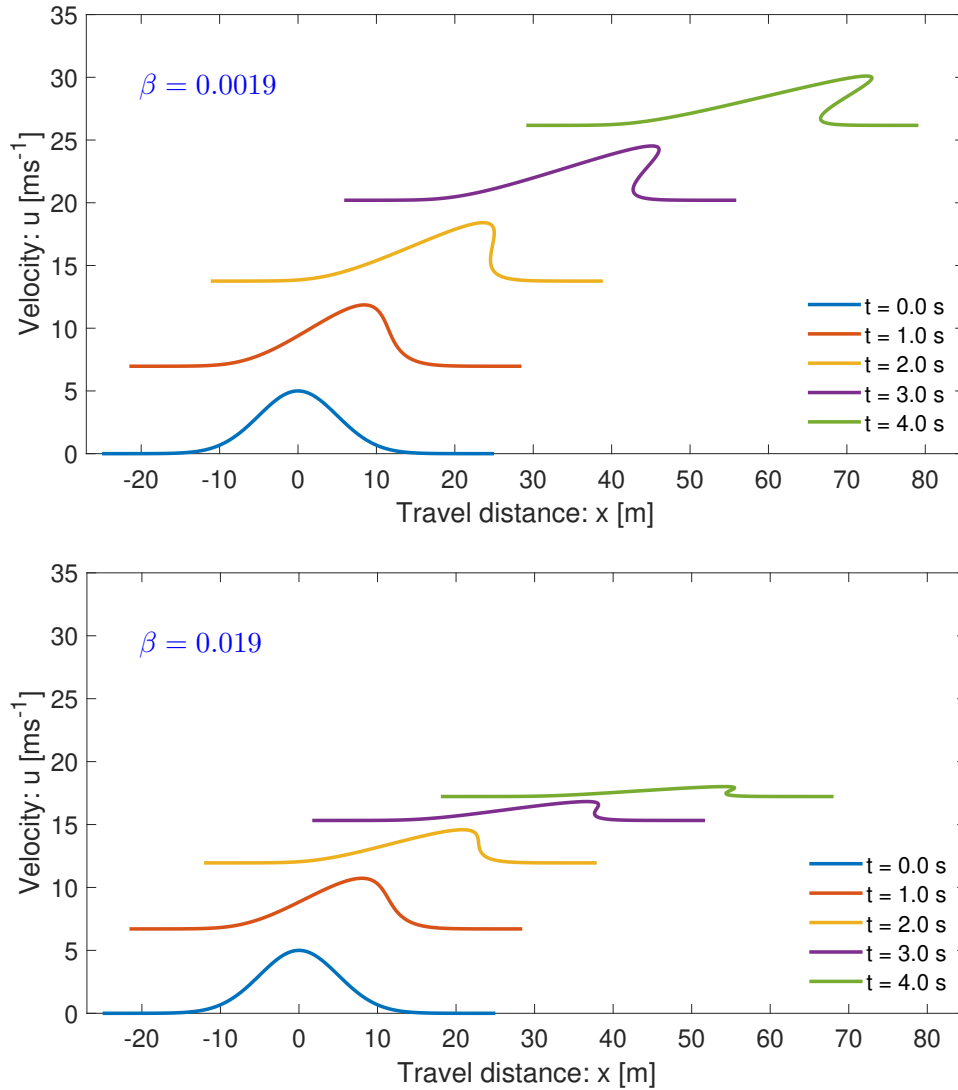


Figure 14: The breaking wave and folding as a landslide propagates down a slope. The top panel with lower drag $\beta = 0.0019$, while the bottom panel with higher drag, $\beta = 0.019$, which showing the drag strongly controls the wave breaking and folding, and also the magnitude of the landslide velocity.

681 Burgers' equation. In fact, as shown in Fig. 15, this has exactly happened. For this, the solution domain
 682 remains fixed, and the solution are not uplifted. This proves that Burgers' equation is a special case of our
 683 model (5).

684 5.10 The viscous drag effect

685 It is important to understand the dynamic control of the viscous drag on the landslide motion. For this, we set
 686 $\alpha \rightarrow 0$, but increased the value of the viscous drag parameter by one and two orders of magnitude. The results
 687 are shown in Fig. 16. In connection to Fig. 15, there are two important observations. First, the translation and
 688 stretching of the domain is solely dependent on the net driving force α , and when it is set to zero, the
 689 domain remains fixed. Second, the viscous drag parameter β effectively controls the magnitude of the velocity
 690 field and the wave breaking. Depending on the magnitude of the viscous drag coefficient, the generation of
 691 the shock wave and the wave breaking can be dampened (top panel) or fully controlled (bottom panel). The
 692 bottom panel further reveals, that with properly selected viscous drag coefficient, the new model can describe

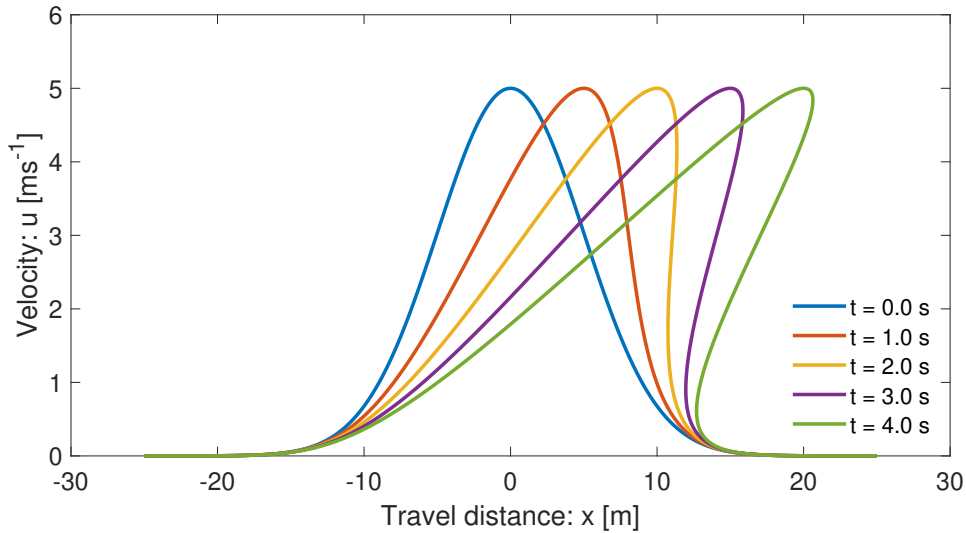


Figure 15: Recovering the Burgers' shock formation and breaking of the wave by the solution system (39)-(40) of the new model (5) in the limit of the vanishing external forcing, i.e., $\alpha \rightarrow 0, \beta \rightarrow 0$.

693 the deposition process of the mass transport and finally brings it to a standstill. In contrast to the classical
 694 inviscid Burgers' equation, due to the viscous drag effect, our model (5) is dissipative, and can be recognized
 695 as a dissipative inviscid Burgers' equation. However, here the dissipation is not due to the diffusion but due to
 696 the viscous drag.

697 6 Discussions

698 **Exact** analytical solutions of the underlying physical-mathematical models significantly improve our knowledge
 699 of the basic mechanism of the problem. On the one hand, **such exact, analytical** solutions disclose many
 700 new and essential physics, and thus, may find applications **broadly** in environmental and engineering mass
 701 transports down natural slopes or industrial channels. The reduced and problem-specific solutions provide
 702 important insights into the full behavior of the complex landslide system, mainly the landslide motion with non-
 703 linear internal deformation together with the external forcing. On the other hand, exact analytical solutions
 704 to simplified cases of non-linear model equations are necessary to calibrate numerical simulations (Chalfen
 705 and Niemiec, 1986; Pudasaini, 2011, 2016; Ghosh Hajra et al., 2018). For this reason, this paper is mainly
 706 concerned about the development of a new general landslide velocity model and construction of several novel
 707 exact analytical solutions for landslide velocity.

708 Analytical solutions provide the fastest, cheapest, and probably the best solution to a problem as measured
 709 from their rigorous nature and representation of the dynamics. Proper knowledge of the landslide velocity
 710 is required in accurately determining the dynamics, travel distance and enormous destructive impact energy
 711 carried by the landslide. The velocity of a landslide is associated with its internal deformation (inertia) and the
 712 externally applied system forces. The existing influential analytical landslide velocity models do not include
 713 many important forces and internal deformation. The classical analytical representation of the landslide velocity
 714 appear to be incomplete and restricted, both from the physics and the dynamics point of view. No velocity
 715 model has been presented yet that simultaneously incorporates inertia and the externally applied system forces
 716 that play crucial role in explaining important aspects of landslide propagation, motion and deformation.

717 We have presented the first-ever, physics-based, analytically constructed simple, but more general landslide
 718 velocity model. There are two main collective model parameters: the net driving force and drag. By rigorous
 719 derivations of the exact analytical solutions, we showed that incorporation of the non-linear advection and
 720 external forcing is essential for the physically correct description of the landslide velocity. In this regard, we

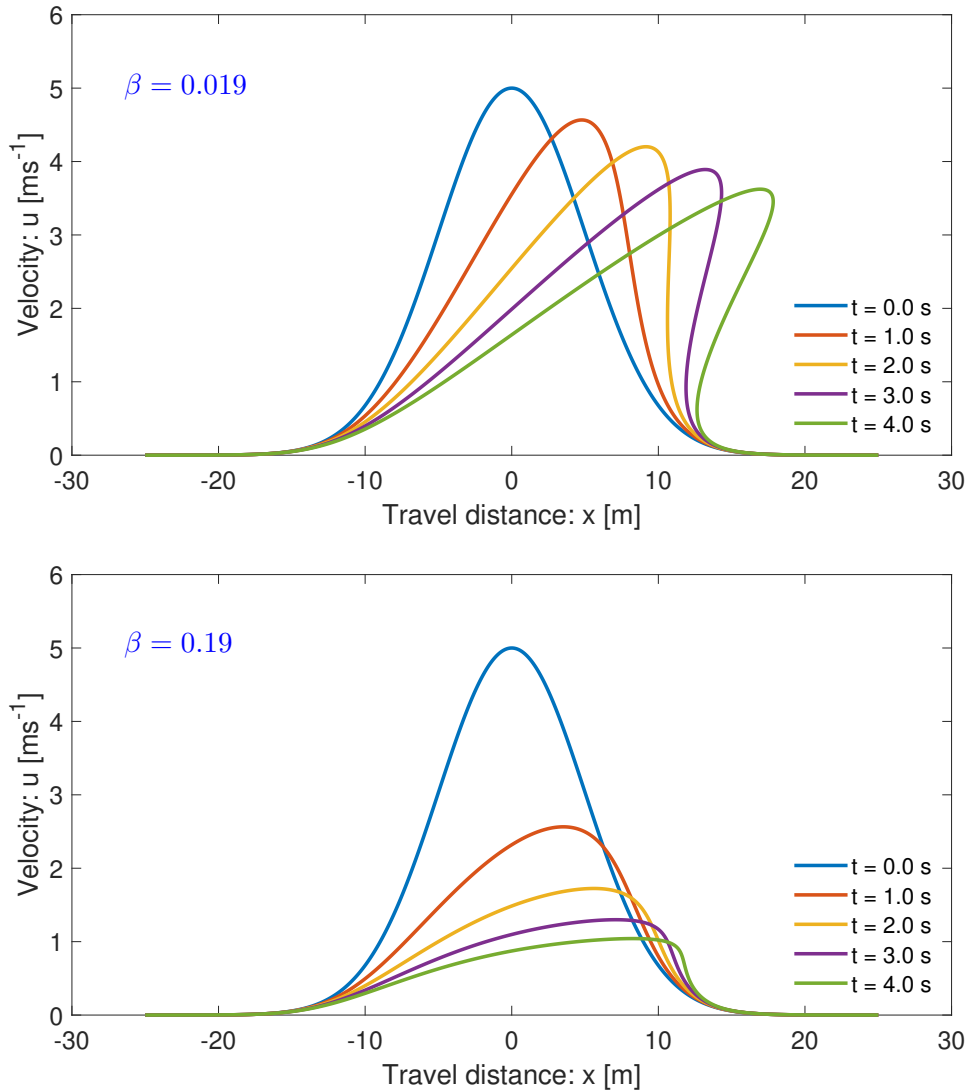


Figure 16: The control of the viscous drag on the dynamics of the landslide. The net driving force is set to zero, i.e., $\alpha = 0$. The viscous drag has been amplified by one and two orders of magnitudes in the top ($\beta = 0.019$) and bottom ($\beta = 0.19$) panels, showing dampened or complete prevention of shock formation and wave breaking, respectively.

721 have presented a novel dynamical model for landslide velocity that precisely explains both the deformation and
 722 motion by quantifying the effect of non-linear advection and the system forces.

723 Different exact analytical solutions for landslide velocity constructed in this paper independently support each
 724 other. **and are compatible with the physics of landslide motion.** These physically meaningful solutions can
 725 potentially be applied to calculate the complex non-linear velocity distribution of the landslide. Our new
 726 results reveal that solutions to the more general equation for the landslide motion are **widely applicable. wide-**
 727 **ranging and include the classical mass point Voellmy and Burgers models for mass transport as special cases.**
 728 The new landslide velocity model **and** its advanced exact solutions made it possible now to analytically
 729 study the complex landslide dynamics, including non-linear propagation, stretching, wave breaking and folding.
 730 Moreover, these results clearly indicate that the proper knowledge of the model parameters α and β is crucial
 731 in reliable prediction of the landslide dynamics.

732 6.1 Advantages of the new model and its solutions

733 The new model may describe the complex dynamics of many extended physical and engineering problems
734 appearing in nature, science and technology - connecting different types of complex mass movements and
735 deformations. Specifically, the advantage of the new model equation is that the more general landslide velocity
736 can now be obtained explicitly and analytically, that is very useful in solving relevant engineering and applied
737 problems and has enormous application potential. **Broadly speaking, this is the first-ever physics-based model**
738 **to do so.**

739 There are three distinct situations in modelling the landslide motion: (i) The spatial variation of the flow
740 geometry and velocity can be negligible for which the entire landslide effectively moves as a mass point without
741 any local deformation. This refers to the classical Voellmy model. (ii) The geometric deformation of the
742 landslide can be parameterized or neglected, however, the spatial variation of the velocity field may play a
743 crucial role in the landslide motion. In this circumstance, the landslide motion can legitimately be explained
744 by the full form of the new landslide velocity equation (5). The constructed general solutions (19) and (39) -
745 (40) of this model have revealed many important features of the dynamically deforming and advecting landslide
746 motions. (iii) Both the landslide geometry and velocity may substantially change locally. Then, no assumptions
747 on the spatial gradient of the geometry and velocity can be made. For this, only the full set of the basic model
748 equations (1) - (2) can explain the landslide motion. While models and simulation techniques for situations (i)
749 and (iii) are available in the literature, (ii) is entirely new, both physically and mathematically. It is evident
750 that dynamically (ii) plays an important role, first in making the bridge between the two limiting solutions, and
751 second, by providing **the fastest, cheapest and the most efficient solution. of the underlying problem.** Solutions
752 (19) and (39)-(40) include the local deformation associated with the velocity gradient. However, except for
753 parameterization, (19) and (39)-(40) do not explicitly include the geometrical deformation. As long as the
754 spatial change in the landslide geometry is insignificant, we can use (19) or (39)-(40) to describe the landslide
755 motion. These solutions also include mass point motions, and are valid before the fragmentation and/or the
756 significant to large **large** geometric deformations. However, when the geometric deformations are significant,
757 we must use (1) and (2) and solve them numerically with some high resolution numerical methods (Tai et al.,
758 2002; Mergili et al., 2017, 2020a,b).

759 The model (19) or (39)-(40) and (1)-(2) are amicable and can be directly coupled. Such a coupling between
760 the geometrically negligibly- or slowly- deforming landslide motion described by (19) or (39)-(40) and the full
761 dynamical solution with any large to catastrophic deformations described by (1)-(2) is novel. First, this allows
762 us to consistently couple the negligible or slowly deformable landslide with a fast (or, rapidly) deformable
763 flow-type landslide (or, debris flow). Second, our method provides a very efficient simulation due to instant
764 exact solution given by (19) or (39)-(40) prior to the large external geometric deformation that is then linked
765 to the full model equations (1)-(2). The computational software such as r.avaflow (Mergili et al., 2017, 2020a,
766 2020b; Pudasaini and Mergili, 2019) can substantially benefit from such a coupled solution method. Third,
767 importantly, this coupling is valid for single-phase or multi-phase flows, because the corresponding model (5)
768 is derived by reducing the multi-phase mass flow model (Pudasaini and Mergili, 2019).

769 Burgers' equation has no external forcing term. The solution domain remains fixed and does not stretch and
770 propagate downslope. So, the initial velocity profile deforms and the wave breaks within the fixed domain.
771 In contrast, our model (5) is fundamentally characterized and explained simultaneously by the non-linear
772 advection $u\partial u/\partial x$ and external forcing, $\alpha - \beta u^2$. The first designs the main dynamic feature of the wave, while
773 the later induces rapid downslope propagation, stretching of the wave domain and quantification of the wave
774 form and magnitude. These special features of our model are often observed phenomena in mass transport,
775 and are freshly revealed here.

776 6.2 Compatibility, reliability and generality of the solutions

777 Within their scopes and structures, many of the analytical solutions constructed in Sections 3 - 5 are similar.
778 This effectively implies the physical aspects of our general landslide velocity model (5), and also the compat-
779 ibility and reliability of all the solutions. **We have seen that** The solutions (19) and (39)-(40) recover all the

780 mass point motions given by (11) and (13). **However, the analyses presented in Sections 3 - 5 reveal that** From
781 the physical and dynamical point of view, the velocity profiles given by (19) and (39)-(40) as solutions of the
782 general model for the landslide velocity (5) are much wider and better than those given by (11) and (13) as
783 solutions of the mass point model (10).

784 Structurally, the solutions presented in Section 3 are only partly new, yet they are physically substantially
785 advanced. However, in Section 4 and 5 we have presented entirely novel solutions, both physically and struc-
786 turally. From physical and mathematically point of view, particularly important is the form of the general
787 velocity model (5). First, it extends the classical Voellmy mass point model (Voellmy, 1955) by including: (i)
788 much wider physical aspects of landslide types and motions, and (ii) the landslide dynamics associated with
789 the internal deformation as described by the spatial velocity gradient associated with the advection. Second,
790 the model (5) is the direct extension of the inviscid Burgers' equation by including a (quadratic) non-linear
791 source as a function of the state variable. This source term contains all the applied forces appearing from the
792 physics and mechanics of the landslide motion.

793 Moreover, as viewed from the general structure of the model (5), all the solutions constructed here can be
794 utilized for any physical problems that can be cast and represented in the form (5), but independent of the
795 definition of the model parameters α and β , **and the state variable u (Faraoni, 2022).** **These parameters, and**
796 **the initial (or, boundary) condition are dependent on the physics of the problem under consideration.**

797 **6.3 Importance and Implications**

798 **A further important feature is the construction of the general and particular exact analytical solutions to the**
799 **model (5) and the description of their physical significance and application in quickly and efficiently solving**
800 **technical problems. So, in short,** The new model (5) and its solutions have broad implications, mathematically,
801 physically and technically. By deriving a general landslide velocity model and its various analytical exact solu-
802 tions, we made a breakthrough in correctly determining the velocity of a deformable landslide that is controlled
803 by several applied forces as it propagates down the slope. We achieve a novel understanding that the inertia and
804 the forcing terms ultimately regulate the landslide motion and provide physically more appropriate analytical
805 description of landslide velocity, dynamic impact and inundation. This addresses the long-standing scientific
806 question of explicit and full analytical representation of velocity of deformable landslides. Such a description
807 of the state of landslide velocity is innovative.

808 As the analytically obtained values well represent the velocity of natural landslides, technically, this provides
809 a very important tool for the landslide engineers and practitioners in quickly, efficiently and accurately de-
810 termining the landslide velocity. The general solutions presented here reveal an important fact that accurate
811 information about the mechanical parameters, state of the motion and the initial condition is very important for
812 the proper description of the landslide motion. We have extracted some interesting particular exact solutions
813 from the general solutions. As direct consequences of the new general solutions, some important and non-
814 trivial mathematical identities have been established that replace very complex expressions by straightforward
815 functions.

816 **7 Summary**

817 **While existing analytical landslide velocity models cannot deal with the internal deformation and mostly fail to**
818 **integrate a wide spectrum of externally applied forces, we developed a simple but general analytical model that**
819 **is capable of including both of these important aspects. In this paper, we (i) derived a general landslide velocity**
820 **model applicable to different types of landslide motions with internal deformations, and (ii) solve it analytically**
821 **to obtain several exact solutions as a function of space and time for landslide motion, and highlight the essence**
822 **of the new model to enhance our understanding of landslide dynamics. The model is developed by reducing**
823 **a multi-phase mass flow equations (Pudasaini and Mergili, 2019) and includes the internal (local) deformation**
824 **due to non-linear advection (inertia), and the external forcing consisting of the extensive net driving force**
825 **and viscous drag. The model describes a dissipative system and involves dynamic interactions between the**

826 advection and external forcing that control the landslide deformation and motion. In the form, our model
827 constitutes a unique and new class of non-linear advective - dissipative system with quadratic external forcing
828 as a function of state variable, containing all system forces. The new model is a more general formulation, but
829 can also be viewed as an extended inviscid, non-homogeneous, dissipative Burgers' equation. The form of the
830 new equation is important as it may describe the dynamical state of many extended physical and engineering
831 problems appearing in nature, science and technology. From the physical and mathematical point of view,
832 there are two crucial novel aspects: First, it extends the classical Voellmy model due to the broad physics
833 carried by the model parameters and additionally explains the dynamics of deforming landslide described by
834 advection. So, our model provides a better and more detailed picture of the landslide motion by including the
835 local deformation. Second, it extends the classical inviscid Burgers' equation by including the non-linear source
836 term, as a quadratic function of the field variable. The source term accommodates the mechanics of underlying
837 problem through the physical parameters, the net driving force and the dissipative viscous drag.

838 Due to the non-linear advection and quadratic forcing, the new general landslide velocity model poses a great
839 mathematical challenge to derive explicit analytical solutions. We focused on constructing several new and
840 general exact analytical solutions in more sophisticated forms. These solutions are strong, recover all the mass
841 point motions and provide much wider spectrum for the landslide velocity than the classical Voellmy and
842 Burgers' solutions. We have illustrated that the new system of solutions generalize the mass point motion in
843 many different ways. The major role is played by the non-linear advection and system forces. The general
844 solutions provide essentially new aspects in our understanding of landslide velocity. We have analytically
845 proven that after a sufficiently long distance or time, the net driving force and drag always maintain a balance,
846 resulting in the terminal velocity. We have also presented a new model for the viscous drag as the ratio between
847 one half of the system-force and the relevant kinetic energy.

848 With the general solution, we revealed that different classes of landslides can be represented by different
849 solutions under the roof of one velocity model. General solutions allowed us to simulate the progression and
850 stretching (deforming) of the landslide as it slides down. Such deformation stems from the non-linear advection
851 in our primary model. This proves our hypothesis on the importance of advection term on the deformation
852 and motion. The mechanisms of advection, stretching and approaching to the steady-state have been explained
853 with reference to the general solution. We disclose the fact that the shifting and stretching of the velocity field
854 stem from the external forcing and non-linear advection. Also after a long time, as drag strongly dominates
855 the system forces, the velocity approaches the steady-state, practically the velocity gradient vanishes, and thus,
856 the stretching ceases. Then, the landslide propagates down the slope just at a constant velocity.

857 We have shown, that the general solution system can generate complex breaking waves in advective mass
858 transport and describe the folding process of a landslide. Such phenomena have been presented and described
859 mechanically for the first-time. The most fascinating feature is the dynamics of the wave breaking and the
860 emergence of folding. These have been explained with respect to the intrinsic mechanism of our solution.
861 This happened collectively as the solution system simultaneously introduces three important components of
862 the landslide dynamics: downslope propagation and stretching of the domain, velocity up-lift, and breaking or
863 folding in the frontal part while stretching in the rear. This physically proves that the non-uniform motion is
864 the basic requirement for the development of breaking wave and emergence of the landslide folding. This is a
865 novel understanding. We disclosed the fact that the translation and stretching of the domain, and lifting of
866 the velocity field solely depends on the net driving force. Similarly, the viscous drag fully controls the shock
867 wave generation, wave breaking and folding, and also the magnitude of the landslide velocity. Furthermore,
868 with properly selected system force and viscous drag, the new model can describe the deposition or the halting
869 process of the mass transport. As the external forcing vanishes, general solutions automatically reduce to the
870 classical shock wave generated by the inviscid Burgers' equation but without domain translation, stretching
871 and lifting. So, in contrast to the classical inviscid Burgers' equation, due to the viscous drag, our model
872 is dissipative. This proves that the inviscid Burgers' equation is a special case of our general model. The
873 theoretically obtained velocities are close to the often observed values in natural events including landslides
874 and debris avalanches. This indicates the broad application potential of the new landslide velocity model and
875 its exact analytical solutions in quickly solving engineering and technical problems in accurately estimating the

876 impact force that is very important in delineating hazard zones and for the mitigation of landslide hazards.

877 While existing analytical landslide velocity models cannot deal with the internal deformation and mostly fail
878 to integrate a wide spectrum of externally applied forces, we developed a simple but general analytical model
879 that is capable of including both of these important aspects. In this paper, we (i) derived a general landslide
880 velocity model applicable to different types of landslide motions, and (ii) solve it analytically to obtain several
881 exact solutions as a function of space and time for landslide motion, and highlight the essence of the new model.
882 The model includes the internal deformation due to non-linear advection, and the external non-linear forcing
883 consisting of the extensive net driving force and viscous drag. The model describes a dissipative system and
884 involves dynamic interactions between the advection and external forcing that control the landslide deformation
885 and motion. Our model constitutes a unique and new class of non-linear advective - dissipative system with
886 quadratic external forcing as a function of state variable, containing all system forces. The new equation
887 may describe the dynamical state of many extended physical and engineering problems appearing in nature,
888 science and technology. There are two crucial novel aspects: First, it extends the classical Voellmy model
889 and additionally explains the dynamics of locally deforming landslide providing a better and more detailed
890 picture of the landslide motion. Second, it is a more general formulation, but can also be viewed as an
891 extended inviscid, non-homogeneous, dissipative Burgers' equation by including the non-linear source term, as
892 a quadratic function of the field variable. The source term accommodates the mechanics of underlying problem
893 through the net driving force and the dissipative viscous drag.

894 Due to the non-linear advection and quadratic forcing, the new general landslide velocity model poses a great
895 mathematical challenge to derive explicit analytical solutions. Yet, we constructed several new and general
896 exact analytical solutions in more sophisticated forms. These solutions are strong, recover all the mass point
897 motions in many different ways and provide much wider spectrum for the landslide velocity than the classical
898 Voellmy and Burgers' solutions. The major role is played by the non-linear advection and system forces. The
899 general solutions provide essentially new aspects in our understanding of landslide velocity. We have also
900 presented a new model for the viscous drag as the ratio between one half of the system-force and the relevant
901 kinetic energy.

902 With the general solution, we revealed that different classes of landslides can be represented by different
903 solutions under the roof of one velocity model. General solutions allowed us to simulate the progression and
904 stretching of the landslide. We disclose the fact that the shifting and stretching of the velocity field stem
905 from the external forcing and non-linear advection. After a long time, as drag strongly dominates the system
906 forces, the velocity gradient vanishes, and thus, the stretching ceases. Then, the landslide propagates down the
907 slope just at a constant (steady-state) velocity. The general solution system can generate complex breaking
908 waves in advective mass transport and describe the folding process of a landslide. Such phenomena have been
909 presented and described mechanically for the first-time. The most fascinating feature is the dynamics of the
910 wave breaking and the emergence of folding. This happens collectively as the solution system simultaneously
911 introduces three important components of the landslide dynamics: downslope propagation and stretching of
912 the domain, velocity up-lift, and breaking or folding in the frontal part while stretching in the rear. This
913 physically proves that the non-uniform motion is the basic requirement for the development of breaking wave
914 and emergence of the landslide folding. This is a novel understanding. We disclosed the fact that the translation
915 and stretching of the domain, and lifting of the velocity field solely depends on the net driving force. Similarly,
916 the viscous drag fully controls the shock wave generation, wave breaking and folding, and also the magnitude
917 of the landslide velocity. Furthermore, the new model can describe the deposition or the halting process of the
918 mass transport. As the external forcing vanishes, general solution automatically reduces to the classical shock
919 wave generated by the inviscid Burgers' equation. This proves that the inviscid Burgers' equation is a special
920 case of our general model.

921 The theoretically obtained velocities are close to the often observed values in natural events including landslides
922 and debris avalanches. This indicates the broad application potential of the new landslide velocity model and
923 its exact analytical solutions in quickly solving engineering and technical problems in accurately estimating the
924 impact force that is very important in delineating hazard zones and for the mitigation of landslide hazards.

925 Acknowledgements

926 Shiva P. Pudasaini acknowledges the financial support provided by the Technical University of Munich with
927 the Visiting Professorship Program, and the international research project: AlpSenseRely – Alpine remote
928 sensing of climate-induced natural hazards - from the Bayerisches Staatsministerium für Umwelt und Ver-
929 braucherschutz, Munich, Bayern. We thank the reviewers and the Associate Editor Jens Turowski for their
930 constructive comments and suggestions that helped to substantially improve the paper. This paper is based
931 on: arXiv:2103.10939v1, <https://arxiv.org/pdf/2103.10939.pdf>.

932 Author contributions

933 The physical-mathematical models were developed by SPP who also designed and wrote the paper, interpreted
934 the results and edited the paper through reviews. MK contributed to the discussions of the results with
935 enhanced descriptions to better fit to the broader geosciences audiences.

936 References

- 937 [1] Baselt, I., de Oliveira, G.Q., Fischer, J.-T., Pudasaini, S.P., 2021. Evolution of stony debris flows in
938 laboratory experiments. *Geomorphology*, 372, 107431. <https://doi.org/10.1016/j.geomorph.2020.107431>.
- 939 [2] Berger, C., McArdell, B.W., Schlunegger, F., 2011. Direct measurement of channel erosion by debris flows,
940 Illgraben, Switzerland. *J. Geophys. Res. Earth Surf.* 116, F01002.
- 941 [3] Bertini, L., Cancrini, N., Jona-Lasinio, G., 1994. The Stochastic Burgers Equation. *Commun. Math. Phys.*
942 165, 211-232.
- 943 [4] Burgers, J.M., 1948. A mathematical model illustrating the theory of turbulence. In *Advances in Applied*
944 *Mechanics*, pp 171-199. Academic Press Inc., New York, edited by Richard von Mises and Theodore von
945 Karman.
- 946 [5] Cascini, L., Cuomo, S., Pastor, M., Sorbino, G., Piciullo, L., 2014. SPH run-out modelling of channelized
947 landslides of the flow type. *Geomorphology* 214, 502-513.
- 948 [6] Chalfen, M., Niemiec, A., 1986. Analytical and numerical solution of Saint-Venant equations. *Journal of*
949 *Hydrology* 86(1-2), 1-13.
- 950 [7] Christen, M., Kowalski, J., Bartelt, P., 2010. Ramms: numerical simulation of dense snow avalanches in
951 three-dimensional terrain. *Cold Regions Science and Technology* 63, 1-14.
- 952 [8] Christen, M., Bartelt, P., Gruber, U., 2002. AVAL-1D: an avalanche dynamics program for the practice.
953 In Vol. 2. 1st congress “Interpraevent in the Pacific Rim”, 14 to 18 October 2002. Matsumoto, Japan.
954 Conference proceedings “Protection of habitat against floods, debris flows and avalanches”, pp. 715-725.
- 955 [9] Cole, J.D., 1951. On a quasi-linear parabolic equation occurring in aerodynamics. *Quart. Appl. Math.* 9,
956 225-236.
- 957 [10] Cui, P., Zeng, C., Lei, Y., 2015. Experimental analysis on the impact force of viscous debris flow. *Earth*
958 *Surf. Process. Landf.* 40, 1644-1655.
- 959 [11] Cuomo, S., Pastor, M., Capobianco, V., Cascini, L., 2016. Modelling the space time evolution of bed
960 entrainment for flow-like landslides. *Engineering Geology* 212, 10-20.
- 961 [12] de Haas, T., Nijland, W., de Jong, S.M., McArdell, B.W., 2020. How memory effects, check dams,
962 and channel geometry control erosion and deposition by debris flows. *Scientific Reports.* 10, 14024.
963 <https://doi.org/10.1038/s41598-020-71016-8>.

- 964 [13] de Haas, T., van Woerkom, T., 2016. Bed scour by debris flows: experimental investigation of effects of
965 debris flow composition. *Earth Surf. Process. Landforms* 41, 1951-1966.
- 966 [14] Di Cristo, C., Iervolino, M., Vacca, A., 2018. Applicability of Kinematic and Diffusive models for mud-
967 flows: a steady state analysis. *Journal of Hydrology* 559, 585-595.
- 968 [15] Dietrich, A., Krautblatter, M., 2019. Deciphering controls for debris-flow erosion derived from a liDAR-
969 recorded extreme event and a calibrated numerical model (Rossbichelbach, Germany). *Earth Surf. Process.*
970 *Landform* 44, 1346-1361.
- 971 [16] Dowling, C.A., Santi, P.M., 2014. Debris flows and their toll on human life: a global analysis of debris-flow
972 fatalities from 1950 to 2011. *Nat. Hazards* 71(1), 203-227.
- 973 [17] Erismann, T.H., Abele, G., 2001. *Dynamics of Rockslides and Rockfalls*. Springer, New York.
- 974 [18] Evans, S.G., Bishop, N.F., Smoll, L.F., Murillo, P.V., Delaney, K.B., Oliver-Smith, A., 2009. A re-
975 examination of the mechanism and human impact of catastrophic mass flows originating on Nevado
976 Huascaran, Cordillera Blanca, Peru in 1962 and 1970. *Eng. Geol.* 108, 96-118
- 977 [19] Faug, T., 2015. Depth-averaged analytic solutions for free-surface granular flows impacting rigid walls
978 down inclines. *Phys. Rev. E* 92. <http://dx.doi.org/10.1103/PhysRevE.92.062310>.
- 979 [20] Faug, T., Chanut, B., Beguin, R., Naaim, M., Thibert, E., Baraudi, D., 2010. A simple analytical model
980 for pressure on obstacles induced by snow avalanches. *Ann. Glaciol.* 51 (54), 1-8.
- 981 [21] Faraoni, V., 2022. Helmholtz problem for the Riccati equation from an analogous Friedmann equation. *Eur.*
982 *Phys. J. C* 82, 13. <https://doi.org/10.1140/epjc/s10052-021-09966-0>.
- 983 [22] Frank, F., McArdell, B.W., Huggel, C., Vieli, A., 2015. The importance of entrainment and bulking on
984 debris flow runout modeling: examples from the Swiss Alps. *Nat. Hazards Earth Syst. Sci.* 15, 2569-2583.
- 985 [23] Gauer, P., 2018. Considerations on scaling behavior in avalanche flow along cycloidal and parabolic tracks.
986 *Cold Regions Science and Technology* 151, 34-46.
- 987 [24] Ghosh Hajra, S., Kandel, S., Pudasaini, S.P., 2018. On analytical solutions of a two-phase mass flow model.
988 *Nonlinear Anal. Real World Appl.* 41, 412-427.
- 989 [25] Ghosh Hajra, S., Kandel, S., Pudasaini, S.P., 2017. Optimal systems of Lie subalgebras for a two-phase
990 mass flow. *Int. J. Non-Linear Mech.* 88, 109-121.
- 991 [26] Gubler, H., 1989. Comparison of three models of avalanche dynamics. *Annals of Glaciology* 13, 82-89.
- 992 [27] Havens, S., Marshall, H.-P., Johnson, J.B., Nicholson, B., 2014. Calculating the velocity of a fast-moving
993 snow avalanche using an infrasound array. *Geophys. Res. Lett.* 41, 6191-6198.
- 994 [28] Highland, L.M., Bobrowsky, P., 2008. *The landslide handbook - A guide to understanding landslides:*
995 Reston, Virginia, U.S. Geological Survey Circular 1325, 129 p.
- 996 [29] Hopf, E., 1950. The partial differential equation $u_t + uu_x = \mu u_{xx}$. *Comm. Pure Appl. Math.* 3, 201-230.
- 997 [30] Huggel, C., Zraggen-Oswald, S., Haerberli, W., Kääb, A., Polkvoj, A., Galushkin, I., Evans, S.G.,
998 2005. The 2002 rock/ice avalanche at Kolka/Karmadon, Russian Caucasus: assessment of extraordinary
999 avalanche formation and mobility, and application of QuickBird satellite imagery, *Nat. Hazards Earth*
1000 *Syst. Sci.* 5, 173-187.
- 1001 [31] Iverson, R. M., Ouyang, C., 2015. Entrainment of bed material by earth-surface mass flows: review and
1002 reformulation of depth-integrated theory. *Rev. Geophys.* 53(1), 27-58.

- 1003 [32] Iverson, R.M. , 2012. Elementary theory of bed-sediment entrainment by debris flows and avalanches. *J.*
1004 *Geophys. Res.* 117, F03006.
- 1005 [33] Iverson, R., Reid, M., Logan, M. et al., 2011. Positive feedback and momentum growth during debris-flow
1006 entrainment of wet bed sediment. *Nature Geosci.* 4, 116-121.
- 1007 [34] Johannesson, T., Gauer, P., Issler, D., Lied, K., 2009. In: Barbolini, M., Domaas, U., Harbitz, C.B.,
1008 Johannesson, T., Gauer, P., Issler, D., Lied, K., Faug, T., Naaime, M. (Eds.), *The Design of Avalanche*
1009 *Protection Dams. Recent Practical and Theoretical Developments.* European Commission. Directorate Gen-
1010 eral for Research.
- 1011 [35] Kattel, P., Khattri, K., Pokhrel, P., Kafle, J., Tuladhar, B., Pudasaini, S., 2016. Simulating glacial lake
1012 outburst floods with a two-phase mass flow model. *Annals of Glaciology* 57(71), 349-358.
- 1013 [36] Kattel, P. , Kafle, J. , Fischer, J.-T. , Mergili, M. , Tuladhar, B.M., Pudasaini, S.P., 2018. Interaction of
1014 two-phase debris flow with obstacles. *Eng. Geol.* 242, 197-217.
- 1015 [37] Körner, H.J., 1980. The Energy-Line Method in the Mechanics of avalanches. *J. Glaciology* 26(94), 501-505.
- 1016 [38] Lanzoni, S., Gregoretto, C., Stancanelli, L.M., 2017. Coarse-grained debris flow dynamics on erodible beds.
1017 *J. Geophys. Res. Earth Surf.* 122(3), 592-614.
- 1018 [39] Le, L., Pitman, E.B., 2009. A model for granular flows over an erodible surface. *SIAM J. Appl. Math.* 70,
1019 1407-1427.
- 1020 [40] Li, P., Hu, K., Wang, X., 2017. Debris flow entrainment rates in non-uniform channels with convex and
1021 concave slopes. *J. Hydraul. Res.* 56, 1-12.
- 1022 [41] Liu, W., Yang, Z., He, S., 2021. Modeling the landslide-generated debris flow from formation to propagation
1023 and run-out by considering the effect of vegetation. *Landslides* 18, 43–58.
- 1024 [42] Liu, W., Wang, D., Zhou, J., He, S., 2019. Simulating the Xinmo landslide runout considering entrainment
1025 effect. *Environ. Earth Sci.* 78, 585. doi:10.1007/s12665-019-8596-2.
- 1026 [43] Lu, P.Y., Yang, X.G., Xu, F.G., Hou, T.X., Zhou, J.W., 2016. An analysis of the entrainment effect of
1027 dry debris avalanches on loose bed materials. *SpringerPlus* 5(1), 1621.
- 1028 [44] McClung, D. M., 1983. Derivation of Voellmy’s Maximum Speed and Run-Out Estimates from a Centre-
1029 of-Mass Model. *Journal of Glaciology* 29(102), 350-352.
- 1030 [45] McCoy, S.W., Kean, J.W., Coe, J.A., Tucker, G.E., Staley, D.M., Wasklewicz, T.A., 2012. Sediment
1031 entrainment by debris flows: In situ measurements from the headwaters of a steep catchment. *J. Geophys.*
1032 *Res.* 117, F03016. doi:10.1029/2011JF002278.
- 1033 [46] McDougall, S., Hungr, O., 2005. Dynamic modelling of entrainment in rapid landslides. *Can. Geotech. J.*
1034 42, 1437-1448.
- 1035 [47] Medina, V., Hürlimann, M., Bateman, A., 2008. Application of FLATModel, a 2D finite volume code, to
1036 debris flows in the northeastern part of the Iberian Peninsula. *Landslides* 5, 127-142.
- 1037 [48] Mergili, M., Jaboyedoff, M., Pullarello, J., Pudasaini, S.P., 2020b. Back calculation of the 2017 Piz Cengalo
1038 - Bondo landslide cascade with r.avafflow: what we can do and what we can learn. *Nat. Hazards Earth*
1039 *Syst. Sci.* 20, 505-520.
- 1040 [49] Mergili, M., Pudasaini, S.P., Emmer, A., Fischer, J.-T., Cochachin, A., Frey, H., 2020a. Reconstruction of
1041 the 1941 GLOF process chain at lake Palcacocha (Cordillera Blanca, Peru). *Hydrol. Earth Syst. Sci.* 24,
1042 93-114.

- 1043 [50] Mergili, M., Emmer, A., Juricova, A., Cochachin, A., Fischer, J.-T., Huggel, C., Pudasaini, S.P., 2018.
1044 How well can we simulate complex hydro-geomorphic process chains? The 2012 multi-lake outburst flood
1045 in the Santa Cruz Valley (Cordillera Blanca, Peru). *Earth Surf. Proc. Land.* 43, 1373-1389.
- 1046 [51] Mergili, M., Fischer, J.-T., Krenn, J., Pudasaini, S.P., 2017. *r.avaflow v1*, an advanced open-source com-
1047 putational framework for the propagation and interaction of two-phase mass flows. *Geosci. Model Dev.*
1048 10(2), 553–569.
- 1049 [52] Montecinos, G.I., 2015. Analytic solutions for the Burgers equation with source terms. *arXiv:1503.09079v1*.
- 1050 [53] Nadjafikhah, M., 2009. Exact solution of generalized inviscid Burgers' equation. *arXiv:0908.3601v1*.
- 1051 [54] Perez, S., Aharonov, E., 2015. Long runout landslides: a solution from granular mechanics. *Front. Phys.*
1052 3, 80. doi: 10.3389/fphy.2015.00080.
- 1053 [55] Perla, R., Cheng, T.T., McClung, D.M., 1980. A two-parameter model for snow-avalanche motion. *J.*
1054 *Glaciology* 26(94), 197-207.
- 1055 [56] Pilvar, M., Pouraghniaei, M.J., Shakibaenia, A., 2019. Two-dimensional sub-aerial, submerged, and tran-
1056 sitional granular slides. *Physics of Fluids* 31, 113303. <https://doi.org/10.1063/1.5121881>.
- 1057 [57] Pudasaini, S.P., Krautblatter, M., 2021. The mechanics of landslide mobility with erosion. *Nature Com-*
1058 *munications* 12, 6793 (2021). <https://doi.org/10.1038/s41467-021-26959-5>.
- 1059 [58] Pudasaini, S.P., Fischer, J.-T., 2020. A mechanical erosion model for two-phase mass flows. *International*
1060 *Journal of Multiphase Flow* 132, 103416. <https://doi.org/10.1016/j.ijmultiphaseflow.2020.103416>.
- 1061 [59] Pudasaini, S.P., 2020. A full description of generalized drag in mixture mass flows. *Engineering Geology*
1062 265, 105429. <https://doi.org/10.1016/j.enggeo.2019.105429>.
- 1063 [60] Pudasaini, S.P., Mergili, M., 2019. A multi-phase mass flow model. *Journal of Geophysical Research: Earth*
1064 *Surface*, 124, 2920-2942.
- 1065 [61] Pudasaini, S.P., Ghosh Hajra, S., Kandel, S., Khattri, K.B., 2018. Analytical solutions to a non-
1066 linear diffusion-advection equation. *Zeitschrift für angewandte Mathematik und Physik* 69(6), 150.
1067 <https://doi.org/10.1007/s00033-018-1042-6>.
- 1068 [62] Pudasaini, S.P., 2016. A novel description of fluid flow in porous and debris materials. *Eng. Geol.* 202,
1069 62-73.
- 1070 [63] Pudasaini, S.P., Miller, S.A. , 2013. The hypermobility of huge landslides and avalanches. *Eng. Geol.* 157,
1071 124-132.
- 1072 [64] Pudasaini, S.P., 2012. A general two-phase debris flow model. *J. Geophysics. Res.* 117, F03010.
1073 doi:10.1029/2011JF002186.
- 1074 [65] Pudasaini, S.P., 2011. Some exact solutions for debris and avalanche flows. *Phys. Fluids* 23, 043301.
1075 doi:10.1063/1.3570532.
- 1076 [66] Pudasaini, S.P., Hutter, K., 2007. *Avalanche Dynamics: Dynamics of Rapid Flows of Dense Granular*
1077 *Avalanches*. Springer, Berlin, New York.
- 1078 [67] Qiao, C., Ou, G., Pan, H., 2019. Numerical modelling of the long runout character of 2015 Shenzhen
1079 landslide with a general two-phase mass flow model. *Bull. Eng. Geol. Environ.* 78, 3281-3294.
- 1080 [68] Razis, D., Kanellopoulos, G., der Weele, K., 2018. The granular monoclinical wave. *J. Fluid Mech.* 843,
1081 810-846.

- 1082 [69] Rui, Y., Yin, M., 2019. An Analytical Solution for the Run-Out of Submarine Debris Flows. *Marine*
1083 *Geodesy* 42(3), 246-262.
- 1084 [70] Salm, B., 1966, Contribution to avalanche dynamics. International Symposium on Scientific Aspects of
1085 Snow and Ice Avalanches, 1965, Davos; pp. 199-214: IAHS Publ. No. 69.
- 1086 [71] Saingier, G., Deboeuf, S., Lagree, P.-Y., 2016. On the front shape of an inertial granular flow down a
1087 rough incline. *Physics of Fluids* 28, 053302. <https://doi.org/10.1063/1.4948401>.
- 1088 [72] Schaerer, P.A., 1975. Friction coefficients and speed of flowing avalanches. In: *Snow Mechanics: Proceed-*
1089 *ings of the Grindelwald Symposium, April 1974. Int. Assoc. Sci. Hydro., IAHS-AISH, Pub., 114, 425-432.*
- 1090 [73] Scheidegger, A.E., 1973. On the Prediction of the Reach and Velocity of Catastrophic Landslides. *Rock*
1091 *Mechanics* 5, 231-236.
- 1092 [74] Schürch, P., Densmore, A.L., Rosser, N.J., McArdeell, B.W., 2011. Dynamic controls on erosion and depo-
1093 sition on debris-flow fans. *Geology* 39(9), 827-830.
- 1094 [75] Shugar, D.H., et al., 2021. A massive rock and ice avalanche caused the 2021 disaster at Chamoli, Indian
1095 Himalaya. *Science* 373, 300-306.
- 1096 [76] Tai, Y.-C., Noelle, S., Gray, J.M.N.T., Hutter, K., 2002. Shock-capturing and front-tracking methods for
1097 granular avalanches. *J. Comput. Phys.* 175(1), 269-301.
- 1098 [77] Tai, Y.-C., Gray, J.M.N.T., Hutter, K., Noelle, S., 2001. Flow of dense avalanches past obstructions. *Ann.*
1099 *Glaciol.* 32, 281-284.
- 1100 [78] Theule, J.I., Liebault, F., Laigle, D., Loye, A., Jaboyedoff, M., 2015. Channel scour and fill by debris flows
1101 and bedload transport. *Geomorphology* 243, 92-105.
- 1102 [79] Voellmy, A., 1955. Über die Zerstörungskraft von Lawinen. *Schweizerische Bauzeitung. Jahrg. 73. Ht.*
1103 *12., 159-162; Ht. 15, 212-217; Ht. 17, 246-249; Ht. 19, 280-285. On the destructive force of avalanches,*
1104 *Translation No. 2. Alta. Avalanche Study Center, USDA, Forest Service, 1964.*
- 1105 [80] Walter, F., Amann, S., Kos, A., Kenner, R., Phillips, M., de Preux, A., Huss, M., Tognacca, C.,
1106 Clinton, J., Diehl, T., Bonanomi, Y., 2020. Direct observations of a three million cubic meter rock-
1107 slope collapse with almost immediate initiation of ensuing debris flows. *Geomorphology* 351, 106933.
1108 <https://doi.org/10.1016/j.geomorph.2019.106933>.